Cell Stem Cell

Clinical and Translational Report

Human pallial MGE-type GABAergic interneuron cell therapy for chronic focal epilepsy

Graphical abstract

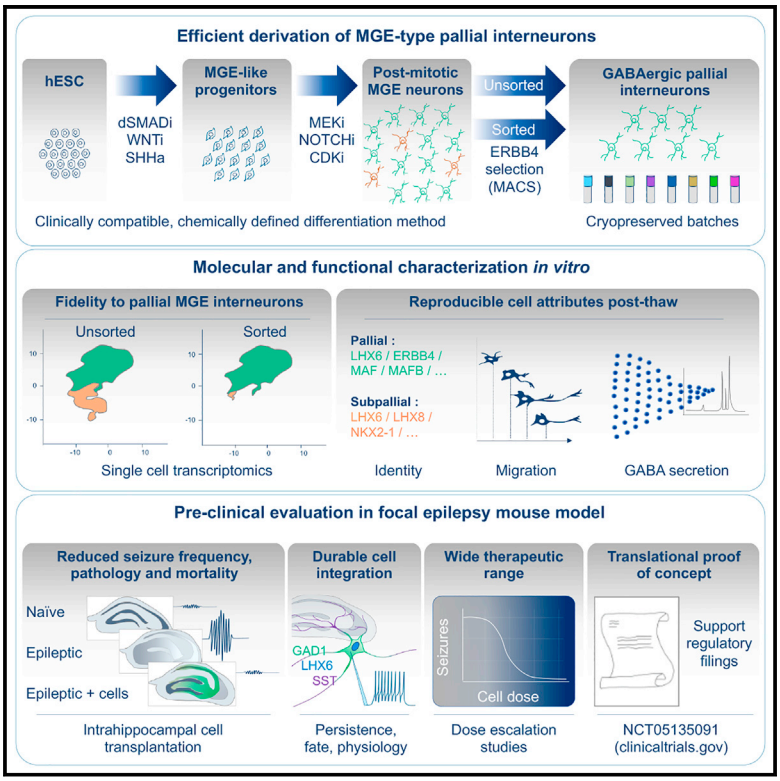

Highlights

- Specific derivation of MGE-type GABAergic pallial interneurons (pINs) from human ESCs
- Post-mitotic human pINs migrate, persist long term, and functionally integrate *in vivo*
- Dose-dependent suppression of seizures and hippocampal pathology in MTLE mouse model
- POC data supporting phase 1/2 clinical trial (NCT05135091) for drug-resistant MTLE

Authors

Marina Bershteyn, Sonja Bröer, Mansi Parekh, ..., Alessandro Bulfone, Catherine Priest, Cory R. Nicholas

Correspondence

cory@neuronatx.com

In brief

Bershteyn and colleagues developed a human GABAergic pallial-type interneuron cell therapy from pluripotent stem cells for the treatment of drug-resistant mesial temporal lobe epilepsy (MTLE). One-time intrahippocampal delivery of human interneurons into a chronic mouse model of MTLE resulted in robust and stable seizure suppression.

Bershteyn et al., 2023, Cell Stem Cell *30*, 1331–1350
October 5, 2023
https://doi.org/10.1016/j.stem.2023.08.013

CellPress

Cell Stem Cell

CellPress
OPEN ACCESS

Clinical and Translational Report

Human pallial MGE-type GABAergic interneuron cell therapy for chronic focal epilepsy

Marina Bershteyn,[1,6] Sonja Bröer,[1,6,7] Mansi Parekh,[1,6] Yves Maury,[1,6] Steven Havlicek,[1] Sonja Kriks,[1] Luis Fuentealba,[1] Seonok Lee,[1] Robin Zhou,[1] Geetha Subramanyam,[1] Meliz Sezan,[1] Eric Steven Sevilla,[1] Whitney Blankenberger,[1] Julien Spatazza,[1] Li Zhou,[2,3] Hubert Nethercott,[1] David Traver,[1] Philip Hampel,[1] Hannah Kim,[1] Michael Watson,[1] Naomi Salter,[1] Anastasia Nesterova,[1] Wai Au,[1] Arnold Kriegstein,[2,3] Arturo Alvarez-Buylla,[3,4] John Rubenstein,[5] Gautam Banik,[1] Alessandro Bulfone,[1] Catherine Priest,[1] and Cory R. Nicholas[1,8,*]

[1]Neurona Therapeutics Inc., South San Francisco, CA 94080, USA
[2]Department of Neurology, University of California, San Francisco, San Francisco, CA 94143, USA
[3]The Eli and Edythe Broad Center of Regeneration Medicine and Stem Cell Research, University of California, San Francisco, San Francisco, CA 94143, USA
[4]Department of Neurological Surgery, University of California, San Francisco, San Francisco, CA 94143, USA
[5]Department of Psychiatry, Weill Institute for Neurosciences, Kavli Institute for Fundamental Neuroscience, University of California, San Francisco, San Francisco, CA 94143, USA
[6]These authors contributed equally
[7]Present address: Institute of Pharmacology and Toxicology, School of Veterinary Medicine, Freie Universität Berlin, Berlin, Germany
[8]Lead contact
*Correspondence: cory@neuronatx.com
https://doi.org/10.1016/j.stem.2023.08.013

SUMMARY

Mesial temporal lobe epilepsy (MTLE) is the most common focal epilepsy. One-third of patients have drug-refractory seizures and are left with suboptimal therapeutic options such as brain tissue-destructive surgery. Here, we report the development and characterization of a cell therapy alternative for drug-resistant MTLE, which is derived from a human embryonic stem cell line and comprises cryopreserved, post-mitotic, medial ganglionic eminence (MGE) pallial-type GABAergic interneurons. Single-dose intrahippocampal delivery of the interneurons in a mouse model of chronic MTLE resulted in consistent mesiotemporal seizure suppression, with most animals becoming seizure-free and surviving longer. The grafted interneurons dispersed locally, functionally integrated, persisted long term, and significantly reduced dentate granule cell dispersion, a pathological hallmark of MTLE. These disease-modifying effects were dose-dependent, with a broad therapeutic range. No adverse effects were observed. These findings support an ongoing phase 1/2 clinical trial (NCT05135091) for drug-resistant MTLE.

INTRODUCTION

Epilepsy, one of the most common central nervous system disorders, is characterized by imbalanced neural excitatory and inhibitory activity, resulting in hyperactive neuronal networks that precipitate and propagate seizures.[1] Systemic administration of anti-seizure drugs (ASDs) largely decreases seizure activity but can be associated with adverse effects,[2,3] and one-third of individuals with epilepsy have drug-resistant seizures.[4–6] Surgical resection or laser ablation can be effective options for some patients with drug-refractory focal epilepsy,[7,8] but these surgeries can cause serious adverse effects, including neurocognitive impairment, and are rarely performed for bilateral mesial temporal lobe epilepsy (MTLE).[9] Thus, development of non-tissue-destructive therapies that target seizure foci, spare surrounding tissue, and avoid ASD-associated toxicities is necessary.

Inhibitory cell therapy could locally restore GABAergic tone to seizure-onset foci and thereby repair underlying pathophysiology. Pallial (commonly referred to as "cortical") GABAergic interneurons (pINs) are the primary source of inhibition in the neocortex and hippocampus (HC). Born in subcortical germinal zones, pINs migrate tangentially to the cortex and HC, where they disperse and acquire mature neurochemical and physiological characteristics.[10–13] Diverse types of pINs are generated by distinct germinal domains in the developing subpallium: the medial ganglionic eminence (MGE) and the nearby preoptic area (POA) generate somatostatin (SST)- and parvalbumin (PV)-expressing pINs, while the caudal ganglionic eminence (CGE) generates 5-Hydroxytryptamine (Serotonin) receptor 3A (HTR3A)-expressing pINs.[11,13–15] Loss of MGE-derived pINs (MGE-pINs) was observed in hippocampal tissues resected from MTLE patients or post-autopsy.[16–19] Furthermore, mutations in genes required for MGE-pIN generation and function have been identified in various developmental epileptic disorders.[20,21] Consistent with these findings, SST and PV pINs are lost or dysfunctional in animal models of epilepsy,[22–24] and seizures can be reduced by their selective activation.[25,26]

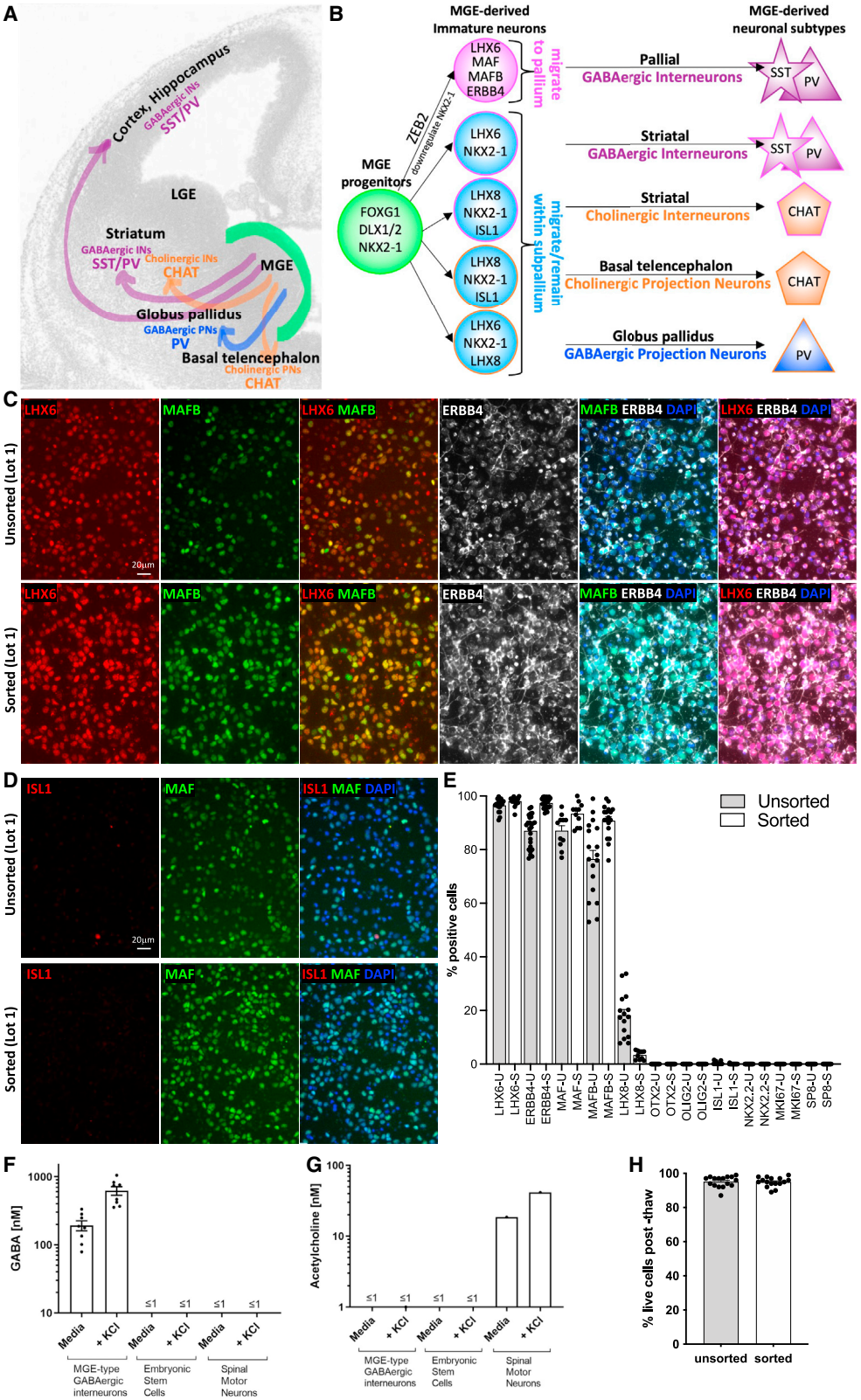

Figure 1. Post-thaw *in vitro* characterization of end-of-process cell lots

(A and B) Simplified schematics of neuronal subtypes derived from the MGE progenitor domain (FOXG1+ DLX1/2+ NKX2-1+), including GABAergic pallial interneurons (pINs) that migrate to the cortex and hippocampus (HC), as well as multiple lineages that remain in the subpallium. The latter include striatal GABAergic

(legend continued on next page)

Proof-of-concept efficacy of MGE-pIN cell therapy has been demonstrated in rodents: transplanted MGE cells dissected from mouse embryonic tissue migrated locally, persisted long term, matured into pINs, functionally integrated with adult circuits,[27,28] and suppressed seizures in rodent models of epilepsy.[29–35] Seizure suppression appeared to be specific to MGE, as CGE transplants did not reduce seizures in epileptic animals and led to disinhibition in wild-type (WT) animals.[36] Thus, the MGE-pINs represent the most anatomically and physiologically relevant GABAergic subclass to pursue for the treatment of MTLE.

Multiple derivation methods for generating MGE-like progenitors and GABAergic neurons from human pluripotent stem cells (hPSCs) have been published.[37–44] Subsequent transplantation studies of hPSC-derived GABAergic neurons into experimental epilepsy models reported promising results of seizure reduction.[45–48] However, despite the widespread use of the term "cortical INs", these cell preparations, based on reported markers and graft phenotypes, appeared to consist of diverse GABAergic populations, including CGE-like INs and non-migratory MGE-like GABAergic projection neurons. Indeed, MGE progenitors are multipotent, producing pINs, GABAergic and cholinergic striatal INs, subpallial projection neurons, oligodendrocytes, and astrocytes.[49–56] Thus, specific derivation of human MGE (hMGE)-pINs from a clinically appropriate source and preclinical evaluation of these cells were lacking. Here, we report the development, characterization, and preclinical evaluation of an hMGE-pIN cell therapy candidate derived from a clinical-grade human embryonic stem cell (hESC) line. The hMGE-pINs were harvested and cryopreserved at a committed post-mitotic, migratory stage of development to mitigate the risks of proliferation and differentiation into undesired cell fates and to ensure local dispersion and circuit integration. Molecular and functional characterization of the pINs is presented, including *in vitro* single-cell RNA sequencing (scRNA-seq), migration, and GABA secretion analyses. Following intrahippocampal transplantation into a chronic mouse model of MTLE, hMGE-pINs were analyzed for migration, persistence, fate, synaptic connectivity, and dose-dependent reduction of seizure activity. The work presented here, using research-grade lots, represents the foundational research that led to investigational new drug (IND) application-enabling studies in support of an ongoing phase 1/2 clinical trial of NRTX-1001 in drug-resistant MTLE (https://www.clinicaltrials.gov/ct2/show/NCT05135091).

RESULTS AND DISCUSSION

Differentiation of hESCs into MGE-pINs

During brain development, NKX2-1+ MGE precursors within the SOX1+, FOXG1+, and DLX1/2+ ventral telencephalon (Figure S1) give rise to multiple neuronal subtypes (Figures 1A and 1B). LHX6 is induced by NKX2-1 in all MGE-derived GABAergic lineages and is largely maintained into adulthood in the SST- and PV-expressing INs within the adult pallium.[57–62] Newborn pINs express tyrosine kinase receptor ERBB4,[63] which is required for tangential migration.[64] In addition, migratory MGE-pINs are distinguished from the other GABAergic lineages by co-expression of LHX6, MAF, and MAFB and downregulation of NKX2-1 and LHX8[60,65–68] (Figure 1B). By contrast, subpallial MGE-derived GABAergic and cholinergic neurons maintain NKX2-1 and/or LHX8 expression and do not express the MAF genes.[51,69] While several studies reported induction of NKX2-1 from hPSCs along with a GABAergic neuron phenotype, they did not demonstrate downregulation of NKX2-1 and LHX8, or co-expression of LHX6 with MAF, MAFB, and ERBB4.

We developed a clinically compatible, 6-week manufacturing protocol using chemically defined reagents to differentiate hESCs into MGE progenitors and subsequently into GABAergic pINs (Figure S2A). After 14 days, over 90% of the cells expressed SOX1, FOXG1, and NKX2-1, and over 80% additionally co-expressed ventricular zone (VZ) marker OTX2, while fewer than 10% expressed LHX6 at this early stage (Figure S1). This combination of markers indicates that day 14 progenitors correspond to a VZ-like MGE stage.

Following initial patterning, kinetics of MGE progenitor, subpallial, and pallial subtype markers were monitored to optimize pIN differentiation. MGE progenitor markers NKX2-1 and OLIG2 increased until week 3 before being downregulated, while LHX6 gradually increased until week 6 along with other markers enriched in pINs, including MAFB, MEF2C, and ERBB4 (Figures S2B–S2G). The fraction of LHX8+ cells initially increased to ~40% during weeks 3 and 4 and then decreased as the cells upregulated LHX6 (Figures S2D and S2E). We found that addition of a Mitogen-activated ERK Kinase (MEK) pathway inhibitor during the MGE progenitor expansion phase promotes pIN differentiation, as evidenced by the downregulation of LHX8 and upregulation of ERBB4 (Figures S2H–S2J). The cholinergic marker ISL1 decreased from 20% at week 2 to less than 1% by week 6 (Figures S2D and S2E; Table S1).

By the end of the differentiation process, ~80% of the hESC-derived cells co-expressed MGE-pIN markers (LHX6, ERBB4, MAF, and MAFB) and the remaining ~20% co-expressed MGE subpallial neuron markers (LHX6 and LHX8) (Figures 1C–1E; Table S1). About one-third of the cells expressed *SST* mRNA (Table S1). Off-target markers, including CGE markers SP8, COUPTF2, and hypothalamic/oligodendrocyte progenitor marker NKX2-2, were not detected (Figures 1E; Table S1; Figures S4D and S4E). Additional bioassays demonstrated that the differentiated neurons secreted the neurotransmitter

and cholinergic INs, cholinergic projection neurons (PN) of the basal telencephalon, and GABAergic PNs of the globus pallidus. Listed genes expressed in the immature neurons play critical roles in the specification of the indicated neuronal subtypes.

(C and D) Representative ICC images of unsorted and sorted lot 1 after cryopreservation and thaw show expression of MGE pIN markers (LHX6, MAFB, MAF, and ERBB4) and cholinergic neurons (ISL1). Scale bar is 20 μm.

(E) Protein quantification across independent lots (n = 10–18).

(F and G) Quantification of (F) GABA and (G) acetylcholine neurotransmitters in the culture supernatant from independent pIN lots (n = 8), undifferentiated hESCs (n = 1), and spinal motor neurons (n = 1).

(H) Cell viability post-thaw from independent pIN lots (n = 16 unsorted/sorted pairs).

In (E)–(H), each dot is an average of technical replicates (2–3) from independently manufactured lots. All data are expressed as a mean ± SEM.

See also Figures S1–S4.

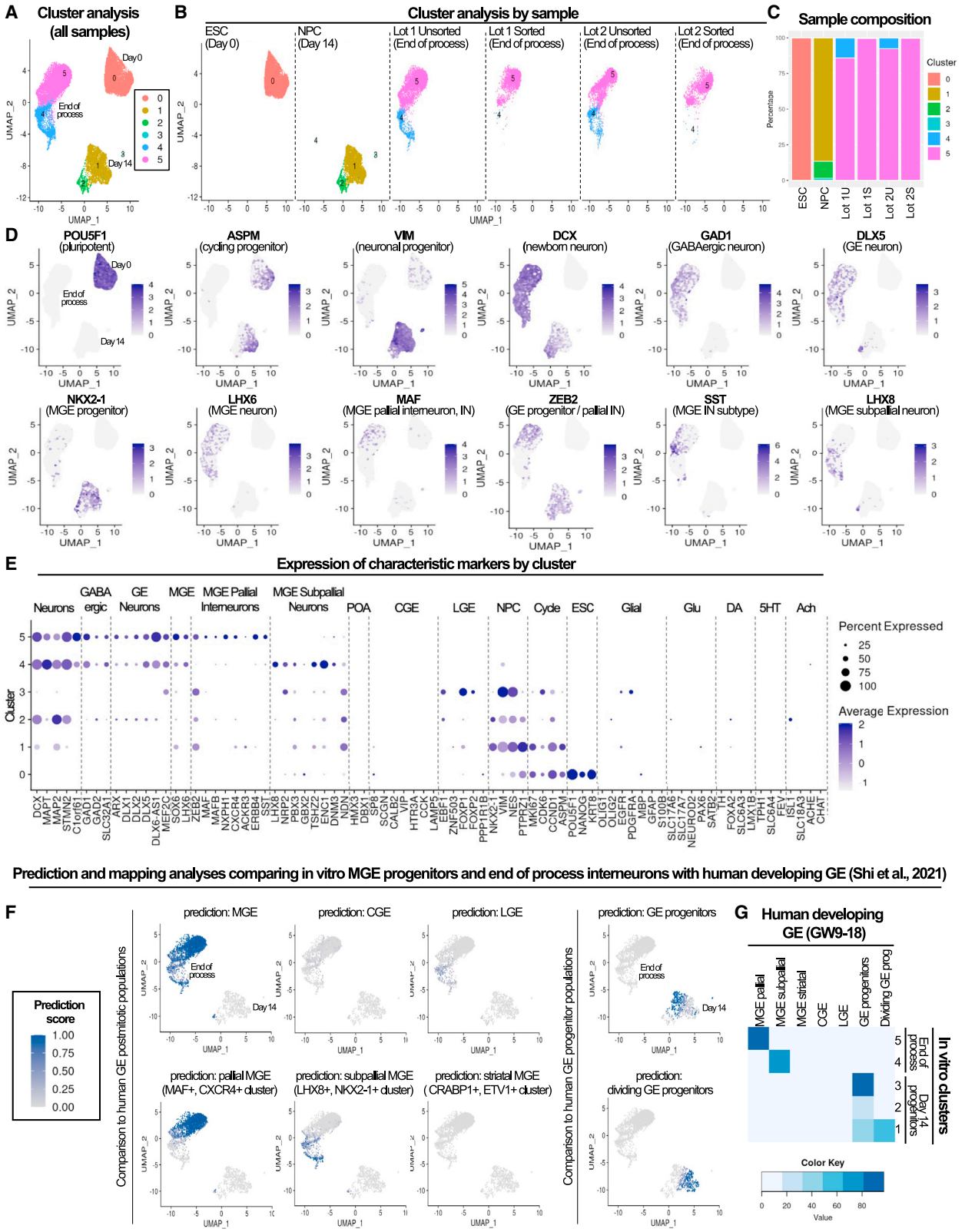

Prediction and mapping analyses comparing in vitro MGE progenitors and end of process interneurons with human developing GE (Shi et al., 2021)

(legend on next page)

GABA, but not acetylcholine (Figures 1F and 1G), and expressed GAD67 protein (93%+) and *VGAT* mRNA (81%+) (Table S1), confirming their GABAergic phenotype.

Previous transplantations of hPSC-derived GABAergic cells gave rise to mixed graft composition with residual cycling cells.[45,46] To avoid potential proliferation and differentiation into off-target cell types, we induced cell-cycle exit and differentiation, using NOTCH and CDK pathway inhibitors during the last phase of the culture (Figure S2A). In the absence of this treatment, a significant proportion of cycling progenitors were still present at week 6. Upon NOTCHi, cycling progenitors were significantly depleted, which was further improved by the addition of CDKi (Figures S3A–S3E). Combined NOTCHi/CDKi treatment also contributed to more rapid downregulation of NKX2-1 and upregulation of LHX6, MAF, and VGAT, consistent with MGE-pIN differentiation (Figures S3E and S3F). Furthermore, analyses of undifferentiated hPSC markers POU5F1 (OCT4) and TRA-1-60 demonstrated absence of residual pluripotent cells by week 2, which was corroborated at the end-of-process (EOP) (Figures S3G–S3I; Figure 2).

To achieve higher purity of MGE-pINs, we performed magnetic purification by positive selection for cells expressing ERBB4. We found that after sorting, the fraction of LHX8+ cells was reduced from ~20% to <5%, while the fraction of cells co-expressing LHX6, MAF, and MAFB increased to >90% (Figures 1C–1E; Table S1). Interestingly, *GAD67* expression and GABA secretion were unaltered upon sorting (Table S1; data not shown), suggesting that the LHX8+ cells are also GABAergic. To facilitate clinical translation, cryopreservation methods were developed to achieve high viability after thawing (Figure 1H). Finally, the migration potential of unsorted and sorted hMGE-pINs was evaluated *in vitro* and compared with the migration of ERBB4-sorted human pINs isolated from fetal MGE as well as two commercial sources of hPSC-derived GABAergic neurons (Figures S4A–S4C). While all the hPSC-derived GABAergic neurons expressed VGAT, only the MGE-pINs expressed high levels of LHX6, MAFB, MAF, and ERBB4 and lacked expression of progenitor (OTX2), glial (GLAST), CGE (COUPTF2 and SP8), and other off-target markers (ISL1 and NKX2-2) (Figures S4B, S4D, and S4E). Furthermore, cell morphology and extent of *in vitro* migration were remarkably similar between the hESC-derived MGE-pINs and the fetal MGE-pINs, which were not recapitulated by the other *in vitro*-derived GABAergic neurons (Figures S4A–S4C). These results indicate functional specificity in the migration assay, which reflects molecular cell identity. Taken together, these data provide evidence for specific, efficient, and reproducible generation of post-mitotic, migratory, GABAergic hMGE-pINs from hPSCs.

scRNA-seq profiling confirms MGE-type GABAergic pIN identity

To objectively characterize cell composition during *in vitro* derivation, scRNA-seq was performed for three stages: day 0 hESCs prior to differentiation, day 14 VZ-like neural progenitor cells (NPCs), and week 6 EOP neurons. Unbiased clustering analysis of all the cells based on global gene expression separated cells by stage and identified six distinct populations (clusters 0–5), representing different cell types and/or states (Figures 2A and 2B). Day 0 hESCs grouped tightly into a single cluster (cluster 0), indicative of homogeneous gene expression in the starting hESC population (Figures 2B and 2C). Pluripotency markers, including *POU5F1* (OCT4) and *NANOG*, were not detected in the NPC-stage samples or the EOP lots (Figures 2D and 2E; Figure S5A). Consistent with flow analyses (Figures S3H and S3I), no residual hPSCs were identified in day 14 NPCs or the EOP lots, regardless of sorting (Figure 2C).

Day 14 NPCs were distributed across three clusters (clusters 1, 2, and 3) (Figures 2A–2C). The two main clusters comprising 98.6% of NPCs (cluster 1%–86.7% and cluster 2%–11.9%) (Figure 2C) were *NKX2-1*+ and *FOXG1*+ and likely represent different MGE precursor maturation states, as evidenced by the inverse gradients of neuronal and progenitor markers. Namely, cluster 1 had higher expression of *NKX2-1* and the radial glia (RG)/NPC markers *VIM*, *NES*, *PTPRZ1*, and *FABP7*. By contrast, cluster 2 had higher expression of neuronal and GABAergic markers *DCX*, *MAP2*, *GAD1/2*, and *DLX1/2/5* (Figures 2D and 2E). These findings are consistent with a transition from VZ-like MGE RG/NPC to more mature secondary progenitors and/or newborn neurons. The remaining minor cluster 3 (1.4% of day 14 cells) appeared to contain *VIM*+ *NES*+ NPCs expressing lateral GE markers (*EBF1*, *FOXP1*, and *FOXP2*; Figure 2E) and barrier-forming fibroblast markers (*LUM*, *COL1A2*, and *DCN*; Figure S5A).[71] Importantly, no cells corresponding to clusters 1/2/3 were identified in the EOP lots, regardless of sorting (Figure 2C). This was also confirmed by the downregulation of MGE progenitor markers, including *NKX2-1*, *VIM*, *NES*, and *PTPRZ1*, and cell-cycle-associated markers *MKI67*, *ASPM*, *CDK6*, and *CCND1* (Figures 2D and 2E), confirming the post-mitotic stage of the EOP cells.

Figure 2. Single-cell RNA sequencing characterization during the differentiation process and comparison with developing human GE

Samples that were sequenced included day 0 hESCs (n = 1), day 14 MGE progenitors (n = 1), and week 6 EOP cells (n = 3 paired unsorted/sorted lots).

(A and B) Uniform manifold approximation and projection (UMAP) visualization of cell clusters (A) in all the samples combined and (B) in each of the separate samples listed.

(C) Quantification of sample composition by cluster.

(D) Feature plots of gene expression. All cells are displayed in light gray, and cells with detectable expression are displayed in purple, with darker shade corresponding to higher expression level.

(E) Dot plot for key genes that define different cell categories, including general markers of neurons, GABAergic and GE neurons, MGE, MGE pINs, MGE subpallial neurons, POA, CGE, LGE, neuronal progenitors (including MGE progenitor marker *NKX2-1*), cell cycle, pluripotent, as well as genes associated with glial cells, glutamatergic neurons (Glu), dopaminergic neurons (DA), serotonergic neurons (5HT), and cholinergic neurons (Ach).

(F and G) Comparison of *in vitro*-derived day 14 progenitors and EOP INs with human developing GE (GW9-18), using the Shi et al. dataset[70] as a reference. (F) Prediction scores between 0 and 1 are projected onto day 14 and EOP UMAP. (G) Heatmap showing percentage of cells in each *in vitro* cluster that are assigned to different GE categories based on prediction scores.

See also Figure S5.

EOP cells were distributed between two main clusters (clusters 4 and 5) (Figures 2B and 2C). Both clusters expressed high levels of the pan-MGE neuron markers *LHX6* and *SOX6* and additional neuronal (*DCX*, *MAPT*, and *MAP2*), GABAergic (*GAD1/2* and *SLC32A1* [VGAT]), and GE markers (*DLX1/2/5*, *DLX6-AS1* [DLX2 co-activator],[72] ARX, and MEF2C) (Figures 2D and 2E). However, cluster 5 had higher expression of genes required for pIN development and migration (*ZEB2*, *MAF*, *MAFB*, *NXPH1*, *SST*, *CXCR4*, *ACKR3* [*CXCR7*], and *ERBB4*), compared with cluster 4 (Figures 2D and 2E; Figure S5A). For example, ZEB2 represses NKX2-1 and is required downstream of DLX1/2 to control the fate switch between striatal (subpallial) and cortical (pallial) INs.[66] Thus, cluster 5 represents the on-target MGE-pIN population, comprising 86% and 92% of cells in the unsorted lots 1 and 2, respectively (Figures 2B and 2C). Over 99% of the cells from the sorted preparations of all sequenced lots corresponded to the on-target MGE-pIN cluster 5 (Figures 2B and 2C). Cluster 4, by contrast, was characterized by co-expression of *LHX6* with *LHX8*, lack of pIN markers, and expression of other genes consistent with subpallial MGE GABAergic projection neurons (*GBX2*, *ENC1*, *DNM3*, and *NDN*)[51,54,73,74] (Figures 2D and 2E; Figure S5A). Cluster 4 comprised 14% and 8% of the population in the unsorted lots 1 and 2, respectively, and less than 1% of the population in the corresponding sorted lots (Figures 2B and 2C). These results are consistent with *in vitro* data presented earlier, suggesting that the main impurities in the unsorted lots are likely MGE-type GABAergic subpallial neurons.

Immature MGE- and CGE-derived pINs ultimately differentiate into transcriptionally heterogeneous IN subtypes, defined, in part, based on expression of calcium-binding proteins (PV (*PVALB*), calbindin/CALB (*CALB1*), and calretinin/CR (*CALB2*)) and neuropeptides (*SST*, neuropeptide Y (*NPY*), vasoactive intestinal peptide (*VIP*), cholecystokinin (*CCK*), and tachykinin precursor 1 (*TAC1*)). It has been shown that SST, NPY, and CCK expression begins in migrating immature pINs during prenatal development.[60,75] Thus, we examined the expression of these and other pIN-subtype markers[61,62,76,77] across samples and clusters (Figures S5B and S5C). Among the markers associated with the MGE-pINs, *PVALB* was not detected, consistent with its known post-natal expression onset,[78] but *SST* transcript was abundant in both unsorted and sorted lots. In addition, other markers expressed by the MGE pINs (*CALB1*, *NPY*, and *RELN*) were detected, particularly in the on-target EOP cluster 5 (Figures S5B and S5C). By contrast, markers that are more abundant in the CGE-derived pINs (*CCK*, *VIP*, *HTR3A*, *CALB2*, *SP8*, and *SCGN*) were not expressed (Figures S5B, S5C, and S2E). There was also no expression of non-specific markers, including ones associated with POA, lateral ganglionic eminence (LGE: striatal/olfactory), glial cells, or other neuronal classes (Figure 2E). Collectively, these findings provide unbiased global transcriptomic validation for the highly specific derivation of post-mitotic, GABAergic MGE-pINs.

To further evaluate *in vitro*-derived cell identity, we compared our day 14 and EOP single-cell gene expression data with a single-nuclei RNA-seq dataset from the human developing ganglionic eminence (GE) (gestational weeks GW9–18).[70] This study captured several post-mitotic MGE populations, including a prominent pallial cluster (Figure S5D, "red": *LHX6*+, *MAF*+, and *CXCR4*+), a subpallial cluster (Figure S5D, "dark blue": *LHX6*+, *LHX8*+, and *NKX2-1*+), and a striatal cluster (Figure S5D, "purple": *LHX6*+, *CRABP1*+, and *ETV1*+). In addition, this dataset included GE progenitors (not annotated by different regions), as well as post-mitotic CGE (Figure S5D, "orange": *SCGN*+ and *CALB2*+) and LGE (Figure S5D, "green and light blue": *MEIS2*+ and *FOXP1*+) populations. We implemented a prediction algorithm, assigning a score between 0 and 1 to each cell based on the transcriptome-wide similarity in gene expression between the query (*in vitro* cells) and the reference (*in vivo* clusters). These unsupervised analyses demonstrated that day 14 progenitors had strong prediction scores for human GE progenitors and not for the post-mitotic MGE populations, and vice versa (Figures 2F and 2G). Furthermore, the EOP cells had very high similarity to human endogenous MGE (Figure 2F), with cells in cluster 5 having strong prediction scores for the pallial MGE cluster and cells in cluster 4 having strong prediction scores for the subpallial MGE cluster (Figures 2F and 2G). We did not identify any hESC-derived cells similar to the striatal MGE cluster from the Shi et al. dataset.[70] Some of the cluster 4 cells had a low prediction score for LGE, likely due to a shared transcriptional program between the two regions.[74] Importantly, none of the hESC-derived cells showed similarity to CGE (Figures 2F and 2G), consistent with the lack of CGE marker expression.

hESC-derived MGE-pINs persist long term and functionally integrate in the wild-type and epileptic rodent pallium

Sorted hMGE-pINs were transplanted into post-natal mouse brain to characterize their electrophysiological properties within the rodent pallium. Prior to transplantation, cells were labeled using a lentivirus expressing either EGFP under the control of the human ubiquitin promoter (hUbC) (Figures 3A–3Q and 3U–3W) or channelrhodopsin (ChR2)-EYFP under the control of the synapsin (SYN) promoter (Figures 3T and 3X–3Z). EGFP-labeled cells were injected bilaterally into the neocortex of post-natal day (P)0–2 mice. Histological assessment of the transplants was performed 2.5 and 5.5 months post-transplant (MPT) (Figures 3A and 3B). From 2.5 to 5.5 MPT, human cells marked by human-specific nuclear and membrane antigen (HNMA) displayed an increasing number of branches (Figure 3A) and maintained LHX6 expression (Figure 3B), thus confirming MGE neuronal lineage.

Electrophysiological properties of the EGFP+ transplanted cells were analyzed at 4 and 7.5 MPT in acute brain slices. Upon recording, cells were backfilled with biocytin and co-stained with human nuclear antigen (HNA) to validate their human origin (Figure 3C). All recorded cells fired action potentials (APs) (Figures 3D and 3E), with 60% and 80% exhibiting spontaneous firing at 4 and 7.5 MPT, respectively. At 7.5 MPT, cells displayed significantly lower mean membrane resistance than at 4 MPT (Figure 3F, $p = 0.0317$) and higher mean membrane capacitance (Figure 3G, $p = 0.0079$), indicative of continued maturation; these values are on par with the values reported by Zhu and colleagues[48] at 10 MPT for *in vitro*-derived GABAergic cells. However, the relatively elevated resting membrane potentials and time constant values (~ -50 mV, Figure 3H; data not shown) indicated that recorded cells were still immature at 7.5 MPT.

CellPress
OPEN ACCESS

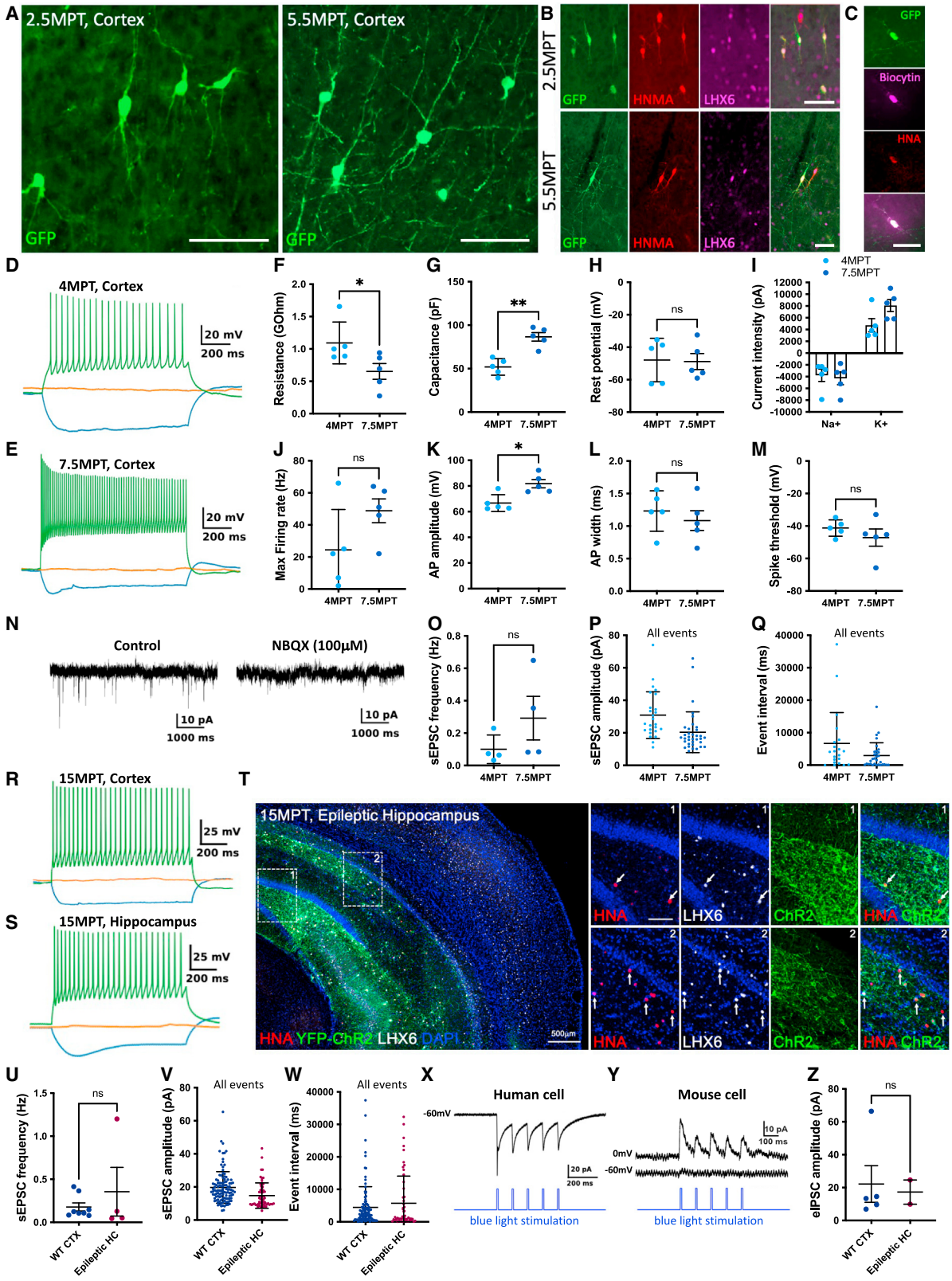

Figure 3. Electrophysiological characterization of grafted human pINs in the rodent pallium

(A) Cell morphology of GFP-labeled human cells at 2.5 and 5.5 months post-transplant (MPT) in the wild-type (WT) mouse cortex.

(B) Immunohistochemistry (IHC) staining with GFP, HNMA, and LHX6.

(legend continued on next page)

Upon voltage pulse application, transplanted cells displayed rapid inward and sustained outward currents, indicative of voltage-gated Na^+ and K^+ channels. An increase in peak K^+ currents was observed between 4 and 7.5 MPT (Figure 3I). AP properties also indicated a slightly more mature phenotype at 7.5 than at 4 MPT, with a noticeable increase in maximum firing frequency (Figure 3J), significantly higher mean AP amplitude (Figure 3K, $p = 0.0317$), and a tendency toward decreased mean AP duration and threshold (Figures 3L and 3M). Importantly, 80% of human INs exhibited inward currents with fast decay kinetics when holding the voltage at −60 mV (Figures 3N–3Q), which were blocked by the AMPA receptor antagonist NBQX. Thus, the grafted INs were synaptically connected, receiving glutamate-mediated spontaneous excitatory postsynaptic currents (sEPSCs) from host neurons.

We further assessed whether hMGE-pINs could survive long term (up to 1.5 years) and form functional synapses not only in the WT cortex (WT CTX) but also in the epileptic HC. All human cells recorded in the CTX and HC fired APs (Figures 3R and 3S). ChR2-EYFP-expressing hMGE-pINs persisted with extensive processes covering the entire epileptic HC (Figure 3T). At these late time points, 80% of transplanted INs in both the WT CTX and epileptic HC exhibited sEPSCs (Figures 3U–3W). Furthermore, upon blue light stimulation, ChR2-expressing human INs showed fast inward currents (Figure 3X), and endogenous mouse neurons could be identified in both the WT CTX and the epileptic HC with light-evoked inhibitory postsynaptic currents (eIPSCs), likely from the human pINs (Figures 3Y and 3Z). Collectively, these results demonstrate that *in vitro*-derived hMGE-pINs can persist long term, functionally integrate into the rodent pallium, receive excitatory synapses from host neurons, and establish inhibitory synapses onto host neurons.

hESC-derived MGE-pINs significantly suppress seizures in the MTLE mouse model

Immunodeficient NOG mice received an intrahippocampal injection of kainate into the dorsal CA1 region (Figure S6A), which induced status epilepticus followed by the development of chronic epilepsy. In the chronic phase, approximately 1 month after kainate injection, two independent surgeries were conducted to transplant human cells and implant an intrahippocampal electroencephalogram (EEG) electrode (Figure 4A; Figure S6B). Animals displayed typical sclerotic HC pathology, including granule cell (GC) dispersion ipsilateral to the kainate injection (Figure S6B). Baseline electrographic mesiotemporal seizures were detected at a frequency of 10–15 per 30-min period by EEG recordings over multiple days at 1 week and 1–2 MPT (Figure S6C). Several studies in this model have shown that mesiotemporal seizures are resistant to commonly prescribed first-line ASDs, such as carbamazepine and levetiracetam.[79–82] Cryopreserved hMGE-pINs were thawed and transplanted along the rostrocaudal axis of the HC in multiple deposit sites (Figure S6B). Lot 1 unsorted (1-U) and sorted (1-S) cells (Figure 2) were evaluated for seizure-modifying activity at 1–2, 5, and 7 MPT. All treatment groups had comparable seizure frequency and cumulative seizure duration at the beginning of the study (Figures 4B–4F). While the vehicle-treated group exhibited a moderate decrease in frequency and cumulative seizure duration at 5 MPT, it was similar to baseline at 7 MPT (Figures 4E and 4F), and none of the vehicle-treated animals became seizure-free (Figure 4F). By contrast, most of the cell-treated epileptic animals became seizure-free by 5 MPT and remained seizure-free at 7 MPT, with significantly reduced cumulative seizure duration (Figures 4C–4F). Significant reduction in seizure activity was observed with unsorted and sorted cells.

Mesiotemporal seizure suppression was reproducible: across five independently manufactured sorted hMGE-pIN lots administered at the same dose (200-K cells/HC), 72% (48/67) of the cell-transplanted animals responded with >75% reduction in seizure frequency, and 59% (40/67) became seizure-free by 6–7 MPT (Figures 4F and 6A; Figure S6D). This effect was stable for the duration of the longest studies (up to 9 MPT; Figure S6D). Consistently, cumulative seizure duration was significantly lower in animals receiving the hMGE-pIN lots (Figure 4E; Figure S6E).

hESC-derived MGE-pINs disperse, innervate the epileptic HC, and express GABAergic MGE subtype markers

A time course of immunohistochemical analyses revealed intrahippocampal migration of the transplanted cells in the MTLE mouse model by 1 MPT, followed by gradual DCX downregulation and SST upregulation from 1 to 8.5 MPT (Figures 4G, 5A, and 5B). At 8.5 MPT, virtually all the human cells were MAP2 positive (Figure 4H), migrated >0.9 mm from the injection sites, and

(C) Example of a biocytin-filled cell co-stained for GFP and HNA.

(D–Q) Whole-cell patch-clamp recordings in acute brain slices at 4 and 7.5 MPT (n = 5 validated human cells from 1 mouse for each time point). (D and E) Examples of action potentials (Aps) recorded from transplanted human pINs at 4.5 and 7.5 MPT. (F–M) Physiological properties, including membrane resistance (F), capacitance (G), resting membrane potential (H), peak intensities for sodium (Na^+) and potassium (K^+) currents (I), maximum AP firing rate (J), maximum AP amplitude (K), AP width (L) and the threshold to spike (M). (N) Example of an inward current detected at −60 mV in the majority of the recorded human cells (n = 4 out of 5 cells for both time points), which was blocked by NBQX. (O) Average sEPSC frequency (n = 4 each). (P and Q) Individual spike amplitudes (P) and inter-spike intervals (Q) recorded from the human cells at 4 and 7.5 MPT.

(R and S) Examples of human pINs firing evoked Aps at ~15 MPT (R) in the WT cortex (WT CTX) (n = 10 cells recorded from 2 mice) and (S) in the HC (n = 5 cells recorded from 1 mouse).

(T) IHC staining for ChR2-YFP, HNA, and LHX6 in the epileptic HC at ~15 MPT. Regions 1 and 2 are shown at higher magnification with arrows pointing out examples of human cells (HNA+ LHX6+).

(U–W) Analysis of sEPSCs detected in the majority of human cells at ~15 MPT in the WT CTX (n = 8 out of 10) and epileptic HC (n = 4 out of 5). (U) Average sEPSC frequency, (V) individual sEPSC amplitudes, and (W) inter-event intervals.

(X–Z) (X) Blue light stimulation was used to induce inward currents in ChR2-expressing human cells, (Y) leading to evoked inhibitory postsynaptic currents (eIPSC) that were measured from the host mouse neurons. (Z) Average eIPSC amplitudes recorded from mouse neurons following blue light stimulation in the WT CTX (n = 5 out of 23 recorded cells from 4 mice, ~17 MPT) and in the epileptic HC (n = 2 out of 4 recorded cells from 1 mouse, ~16 MPT).

Throughout the figure, scale bars represent 100 μm, except in (T) (scale bars, 500 μm); All data are expressed as mean ± SEM. Significant differences are indicated by asterisks (*$p < 0.05$; **$p < 0.01$; ****$p < 0.0001$), Mann-Whitney test.

CellPress
OPEN ACCESS

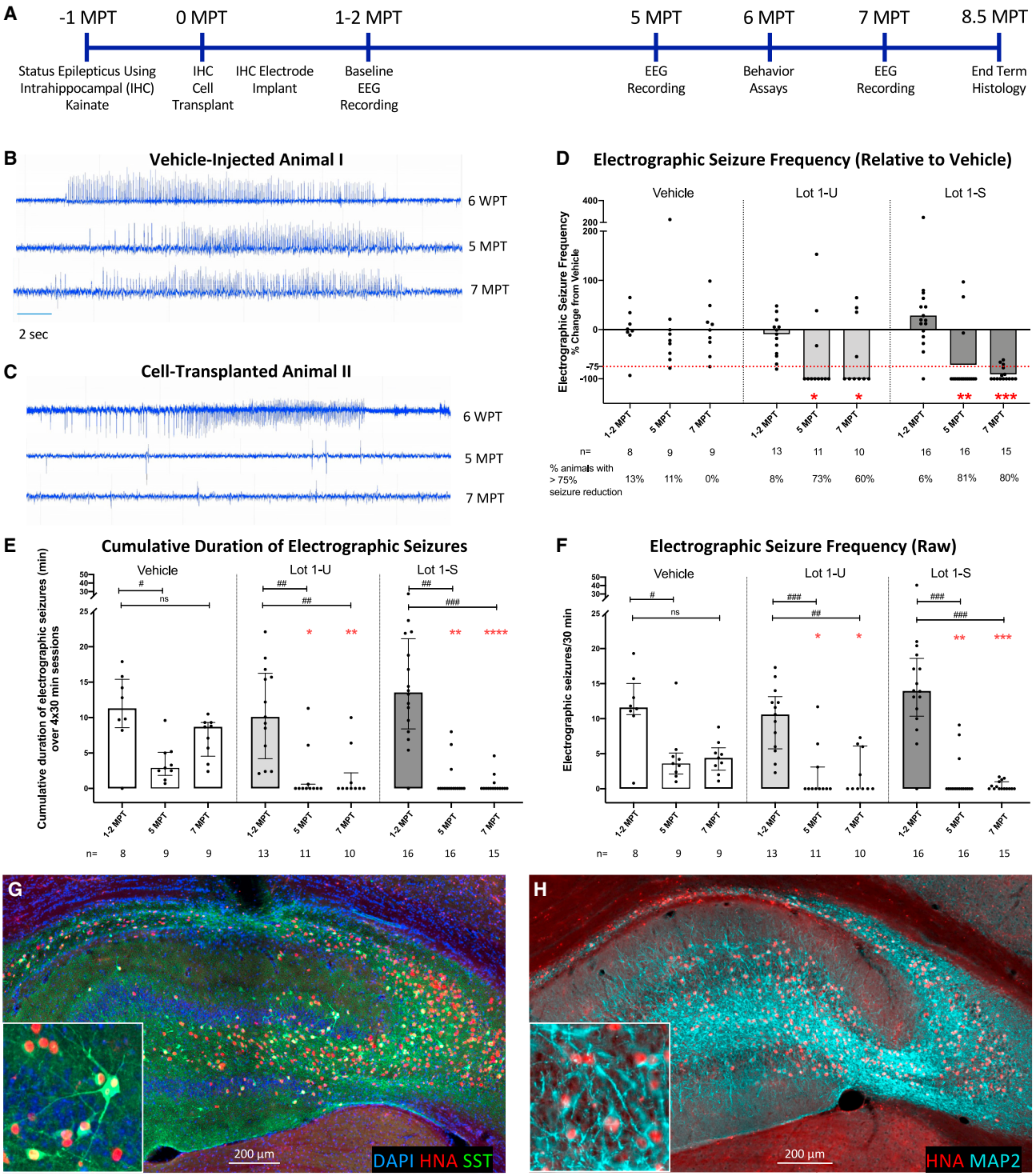

Figure 4. Seizure suppression after cell transplantation of lots 1-U and 1-S in the chronic MTLE mouse model

(A) Experimental timeline.

(B–F) EEG was recorded at the indicated time points post-transplant to detect electrographic seizure frequency and duration. Typical electrographic seizure phenotypes in chronically epileptic mice at 1–2, 5, and 7 MPT (B) after vehicle or (C) cell injection. (D) Seizure frequency for epileptic animals treated with lots 1-U and 1-S. The mean seizure frequency of the vehicle group is normalized to zero at each respective time point (bar graph represents median). The individual animals (dots) are plotted as a percent difference from the mean seizure frequency of the respective vehicle control group. A responder-rate threshold was designated for animals exhibiting >75% reduction vs. vehicle (depicted as red, dashed line). Mann-Whitney test cell vs. vehicle at respective time point; significant differences are indicated by red asterisks (* $p < 0.05$; ** $p < 0.01$; *** $p < 0.001$). (E and F) Raw data corresponding to (D). Cumulative duration of seizures (E) and

(legend continued on next page)

filled the hilus, extending into the pyramidal cell layers and subiculum along the rostrocaudal and dorsoventral axes (Figure 5C; Figure S6F). Grafted cells extended processes throughout the epileptic HC but not in the overlying cortex, as evidenced by human-specific Tau staining (Figure 5C). Cell clusters or cores were not observed.

At the end of the studies, human cell persistence and fate in the epileptic HC were evaluated. Of the 200-K cells injected per HC (lots 1-U and 1-S), 9-K–12-K (4.5%–6%) persisted at 8.5 MPT (Figure 5F). Fluorescence *in situ* hybridization (FISH) for *GAD1* confirmed that the human cells were GABAergic (99%–100%, Figures 5D and 5G; Figure S6G). In addition, the majority of human cells had detectable LHX6 (80%–95%), and approximately 30%–55% had detectable SST expression (Figures 5E and 5G). A fraction of the SST+ cells co-expressed NPY (Figure 5Eiii). PV expression was rare (<1% of human cells, Figure 5Eiv). However, some of the SST-negative cells expressed WFA (Figure 5Ev), a marker of perineuronal net (PNN)-extracellular matrix structures found primarily on fast-spiking PV+ INs,[83] providing additional proof-of-concept evidence that some of the unidentified LHX6+ human cells may develop into PV pINs. CALB was not detected in human cells (Figure 7L). No significant expression of off-target markers was observed, including CGE-associated pIN markers SP8 (data not shown) and CR (Figure 5Evi). MGE progenitor and glial marker OLIG2 was not detected in human cells (Figures 5Evii and 5G). Astrocyte marker GFAP was very rarely observed along the injection tract and not among the dispersed cells, contributing to less than 0.01% of engrafted cells (Figures 5Eviii and 5G). Similarly, virtually no proliferating KI67+ cells were detected (Figures 5Eix and 5G). Neural stem cell and astrocyte marker vimentin (VIM) was detected in the vehicle-treated ipsilateral HC (Figure S6H), likely labeling endogenous reactive astrocytes. Interestingly, VIM staining was markedly lower in the cell-treated epileptic HC, and VIM was not expressed by human cells (Figure S6H), further confirming the lack of neural progenitors in the graft. Collectively, these results are consistent with *in vitro* data and demonstrate that the hESC-derived MGE-pINs do not exhibit continued neurogenesis or proliferation, migrate locally upon transplantation, and differentiate specifically into GABAergic MGE pIN subtypes. Critically, no teratomas or ectopic tissues were observed upon inspection of hematoxylin and eosin (H&E)-stained brain sections from a rostrocaudal review of the tissue of every animal (data not shown).

hMGE-pINs demonstrate dose-dependent seizure suppression

Lot 2 unsorted (2-U) and sorted (2-S) cells (Figure 2) were evaluated for efficacy in the MTLE mouse model across a series of doses: lot 2-U at 25-K, 50-K, 200-K, and 1.5-M cells per HC; and lot 2-S at 200-K and 1.5-M only. The escalating cell-dose treatment cohorts had separate vehicle control groups (low/mid/high) to match the delivery volumes. Mesiotemporal seizure frequency was suppressed in a dose-dependent manner: the 25-K dose was not sufficient, the 50-K dose was partially effective, and the 200-K and 1.5-M cell doses resulted in statistically significant seizure suppression at 7 MPT (lot 2 U; Figure 6A). Of note, 17% of animals with the 25-K cell dose and 44% of animals with the 50-K cell dose displayed >75% seizure suppression, suggesting partial efficacy. With the highest dose of 1.5-M, 89% (8/9) of animals transplanted with lot 2-U and 100% (15/15) of animals transplanted with lot 2-S were seizure-free at 7 MPT (Figure 6A). These results indicate a wide efficacious dosing range for the hMGE-pINs. Histological analyses confirmed that the two higher doses filled the HC more extensively (Figures 6B and 6E). The relative human cell persistence rate was comparable in the range of 25-K to 200-K doses, averaging 7%–10% of the initial dose, but was notably lower at 1.5-M with <2% of the initial dose persisting (Figure 6H), suggesting a possible plateau in the maximum cell number that could be maintained in the host HC. Similar to lot 1 cells, most of the persisting lot 2 cells were LHX6+ (80%–90%) across doses (Figures 6C, 6F, and 6I), and ~20%–30% had detectable SST expression (Figures 6D, 6G, and 6J). Moreover, proliferating/progenitor markers OLIG2, GFAP, and KI67 were below 0.01% for both unsorted and sorted lot 2 transplants (data not shown).

hMGE-pIN transplantation reduces dentate GC dispersion in the epileptic HC

The intrahippocampal kainate mouse model recapitulates sclerotic hippocampal dentate GC dispersion seen in patients with MTLE.[84–86] To quantitatively assess the effects of cell transplantation on GC dispersion, the width and area of the GC layer were measured in the rostral HC (at the level of kainate injection) of naive, vehicle-, and cell-treated epileptic mice that received different doses of lots 2-U and 2-S (Figures 7A–7H). All cell doses significantly reduced GC layer width compared with vehicle treatment (Figure 7G). There was also a dose-dependent effect on the GC layer area, with more significant reduction observed at the two higher doses (Figure 7H). There were no differences in the GC measurements between animals that received unsorted or sorted cell batches, nor between animal groups that received different vehicle volumes (Figures 7G and 7H). IHC analysis showed NEUN and CALB-positive endogenous cells and confirmed reduced GC dispersion in the cell-treated HC. Cleaved caspase 3 (cl-CASP3) demonstrated that host cell death in the epileptic HC was not noticeably different in cell- or vehicle-treated animals (Figures 7I–7L). The reduced GC dispersion observed in the cell-treated animals was not accompanied by an increase in cl-CASP3 labeling, indicating that human pIN transplantation did not induce GC death.

No adverse effects, improved spatial memory, and increased survival after hMGE-pIN transplantation

Dizziness, sedation, and ataxia are the most common adverse effects of systemically administered GABA-potentiating ASDs.

electrographic seizure frequency (F). In addition, significant changes within a treatment group vs. its own baseline are indicated by hashtags (Kruskal-Wallis test followed by Dunn's; #p < 0.05; ##p < 0.01; ###p < 0.001). All data are mean ± SEM.
(G and H) Human cells (HNA+) migrated and dispersed throughout the HC. Expression of (G) IN-subtype marker SST and (H) neuronal marker MAP2 is shown at 8.5 MPT. Scale bar is 200 μm.
See also Figure S6.

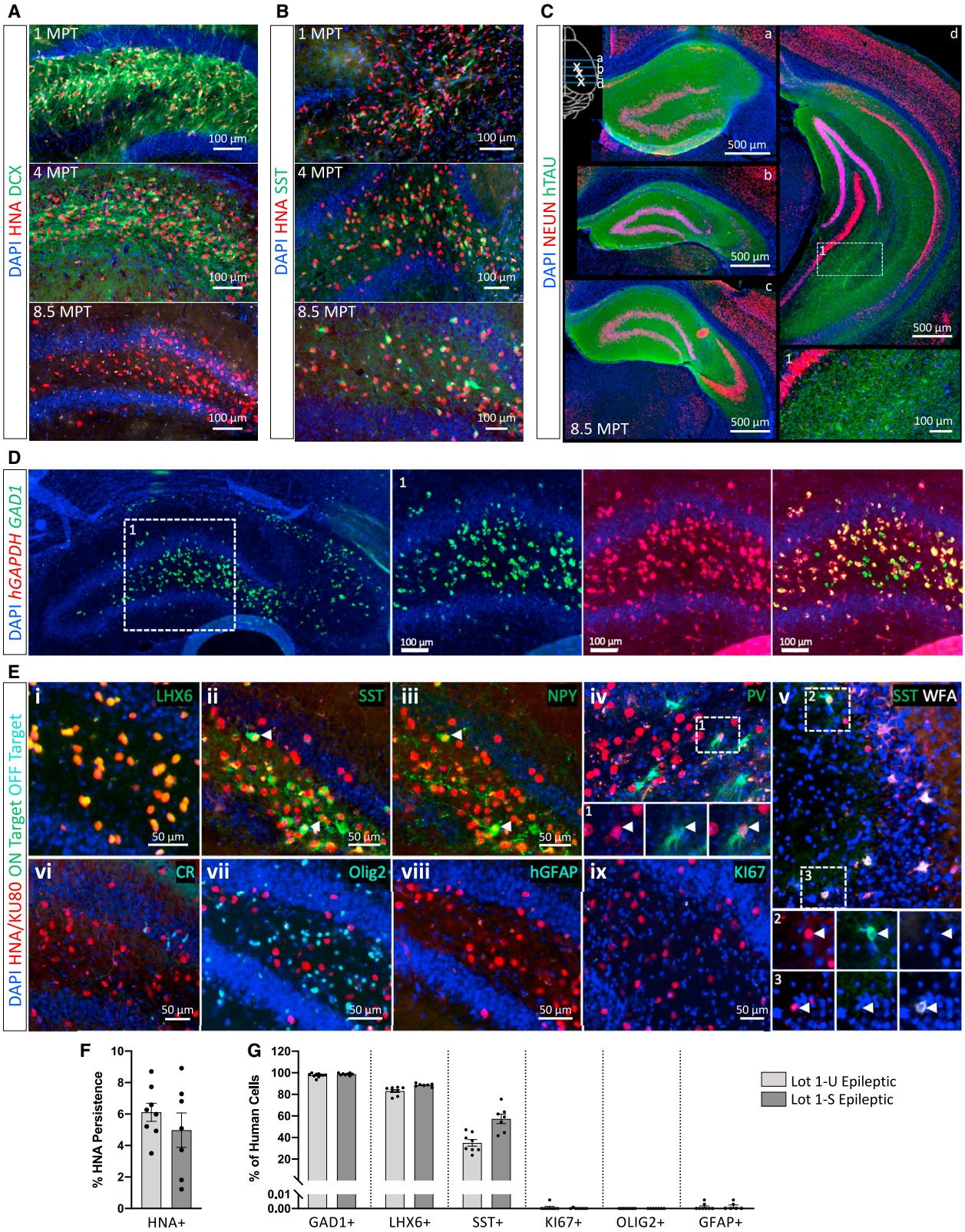

Figure 5. Histological characterization of lots 1-U and 1-S in the epileptic mouse HC

(A and B) Expression of (A) immature neuronal marker doublecortin (DCX) and (B) MGE IN marker SST in human cells (HNA+) at 1, 4, and 8.5 MPT. Scale bars are 100 µm.

(legend continued on next page)

To investigate whether GABAergic hMGE-pINs led to sedative adverse effects, a modified Irwin screen was performed with the epileptic mice that received the highest dose (1.5-M/HC) of lot 2-U. The testing battery included assays for body posture and appearance, excitability, and spatial locomotion (Figure 7M). Cell-transplanted epileptic mice did not show any adverse effects and behaved similarly to the vehicle-treated epileptic mice. Consistent results were found with sorted cells and lower doses (data not shown). Since potential sedative effects could lead to reduced activity, we tested the animals for running velocity in the open field arena and exploratory behavior in the Y-maze. Epileptic vehicle-treated mice ran significantly faster than naive mice, which could be attributed to their hyperexcitability. Activity levels of cell-transplanted mice were not significantly different from that of naive mice (Figure 7N). The preference for left rotations in the Y-maze test (Figure 7O) was seen in vehicle- and cell-treated mice, and it is likely a result of the unilateral kainate injection.[87,88]

A comorbidity of drug-resistant epilepsy, and primary adverse effect of temporal lobe resection/ablation surgery, is impaired learning and memory. Cell-transplanted epileptic mice learned faster in a Barnes maze spatial memory test, compared with vehicle-treated mice, and at a similar rate as naive controls (Figure 7P). Finally, increased mortality is seen in chronically epileptic animals.[89,90] Epileptic animals with high seizure frequency may exhibit deteriorating health requiring euthanasia, or they may die suddenly and unexpectedly, presumably from respiratory arrest or heart failure during a seizure. Significantly improved survival of the epileptic animals was observed after transplantation of 200-K unsorted/sorted cells from lots 1 and 2 (Figure 7Q) and 1.5-M unsorted/sorted cells from lot 2 (data not shown), compared with the vehicle-treated epileptic animals. No difference in survival was observed in mice treated with the lower cell doses (data not shown). In summary, none of the cell doses and lots tested, including the highest dose of 1.5-M unsorted human GABAergic INs per HC, caused behavioral abnormalities, and we observed improvements in learning and memory and increased survival of the cell-treated compared with the vehicle-treated epileptic animals.

Clinical relevance

Worldwide, about 70 million people suffer from epilepsy,[91] and over one-third have drug-resistant seizures. Despite the development of next-generation small molecule ASDs, the proportion of people with pharmacoresistant epilepsy has not changed in decades.[5] Drug-resistant MTLE patients who have a single, well-defined seizure focus may be eligible for a resection or laser ablation surgery. However, these surgeries are destructive to surrounding tissues and can lead to irreversible cognitive deficits. Furthermore, patients with bilateral MTLE are not eligible for bilateral resection/ablation surgery. Thus, there is a medical need to develop safe and effective therapeutics for drug-resistant epilepsy, particularly using strategies that target seizure foci more precisely and are not tissue-destructive.

MGE-pIN loss of function has been implicated in MTLE.[16–19] Therefore, this lineage represents an ideal physiological candidate for targeted cell restoration therapy. Here, we have demonstrated highly efficient and consistent directed differentiation of hESCs into GABAergic MGE-pINs with >85% purity without sorting. Pallial lineage purity was further enriched to >99% using an ERBB4-based purification step. Upon detailed investigation of long-term engraftment, preliminary safety, and disease-modifying activity following intrahippocampal administration into a chronic mouse model of MTLE, both the sorted and unsorted cell lots were comparable in terms of efficacy and safety, suggesting that >85% MGE pIN purity is sufficient, and <15% MGE subpallial GABAergic neuron content is tolerable.

The intrahippocampal kainate mouse model was chosen because of its high face validity to hallmark symptoms of clinical MTLE, i.e., chronic mesiotemporal seizures and hippocampal sclerosis. Recognized as an etiologically relevant model, it is used in the NIH/NINDS-funded Epilepsy Therapy Screening Program,[92] which aims to support progress in the development of new ASDs. High predictive validity can be expected since this model is less responsive to the ASDs commonly prescribed for chronic focal epilepsy, mimicking pharmacoresistant focal epilepsy in patients.[93] However, the model did not produce behavioral impairments as severe as seen in other systemic epilepsy models; thus, our ability to measure behavioral improvements after transplantation is limited.

The total number of surviving human pINs appeared to plateau at higher dose levels, suggesting a compensatory mechanism for regulating inhibitory tone and/or a limitation of maximum engraftable cell number per region of brain tissue. With respect to potential future clinical translation, it is encouraging that similar efficacy was achieved over a wide dosing range from 200-K to 1.5-M pINs per epileptic HC and that no adverse effects were observed.

In addition to long-term cell persistence, dose-dependent suppression of mesiotemporal seizures, and lack of adverse effects in the MTLE model, transplanted hMGE-pINs significantly reduced GC dispersion, a typical pathology of the epileptic HC. Reduced GC dispersion was likely the result of graft-mediated seizure suppression. However, we cannot exclude other mechanisms, such

(C) Human-specific axonal marker hTAU showing transplanted cell processes throughout the epileptic HC (a–d), counter-stained with NEUN. Scale bars are 500 μm.

(D) Grafted human cells were analyzed by FISH using probes against a housekeeping gene for human-specific glyceraldehyde-3-phosphate dehydrogenase (*hGADPH*) and the GABAergic marker glutamate decarboxylase 1 (*GAD1*). Representative image shows cell distribution in the rostral HC with a higher magnification example of the hilus (1). Scale bars are 100 μm.

(E) Representative IHC images showing co-labeling of human cells (HNA+, red) with on-target MGE IN markers in green: LHX6, SST, NPY, and PV, as well as perineuronal nets marker WFA (white). Arrowheads point to specific examples of human cells expressing the markers of interest. Off-target populations including markers for non-MGE lineage INs (CR), oligodendrocytes (OLIG2), human astrocytes (hGFAP), and proliferating cells (KI67) are shown. Scale bars are 50 μm.

(F and G) (F) Quantification of human cell persistence and (G) percent of human cells expressing *GAD1* mRNA, and LHX6, SST, KI67, OLIG2, and GFAP proteins. All data are mean ± SEM.

See also Figure S6.

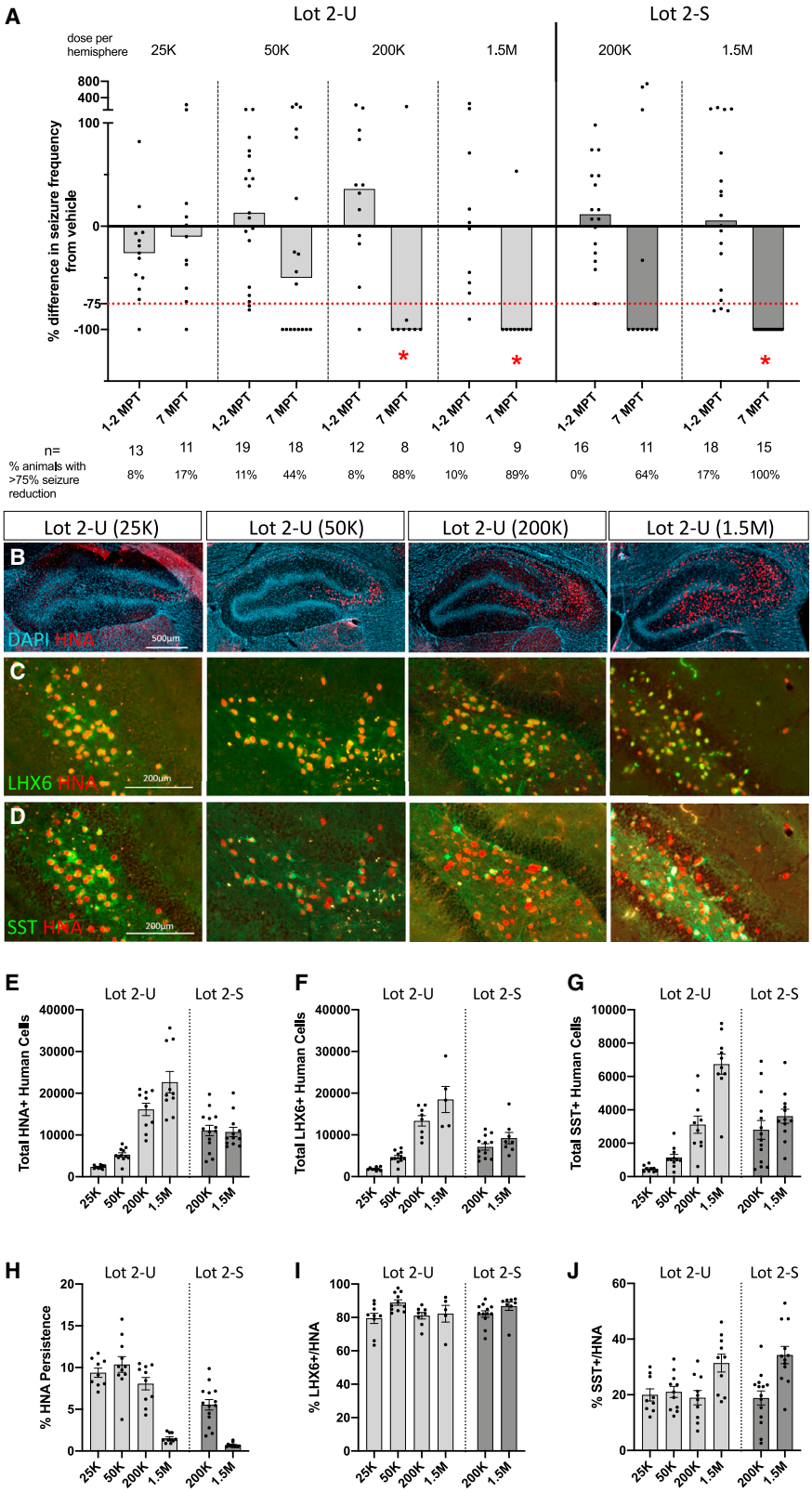

Figure 6. Dose-response seizure suppressing activity of human pINs in the MTLE model

(A) Four doses of unsorted lot 2-U (25-K, 50-K, 200-K, or 1.5-M cells/HC) and two of the higher doses of sorted lot 2-S were evaluated. Vehicle group mean seizure frequency is normalized to zero. Bar graphs represent median, and dots correspond to individual animals. Significant differences between cell vs. vehicle groups

(legend continued on next page)

as the possibility that the transplanted cells promoted regeneration and/or reorganization of the dentate. Future studies will explore the mechanisms leading to reduced HC pathology.

It was also intriguing that mortality was reduced following cell administration. The cause of spontaneous mortality is not always known; however, we have observed animal death immediately following a seizure, similar to sudden unexpected death (SUDEP) in people with epilepsy. Interestingly, epileptic animals treated with hMGE-pINs had reduced mortality by 1–2 MPT, before seizure suppression was observed, suggesting early therapeutic activity, which should be explored further.

Limitations of the study

A significant proportion of the transplanted hMGE-pINs developed into SST+ and NPY+ subtypes by 8.5 MPT. The subtype fate of the remaining GAD1+ LHX6+ hMGE-pINs was not determined in this study and will be resolved in future work. Our preliminary observations suggest that SST protein quantification is an underestimate of the SST subtype content in the grafts, likely due to the protracted accumulation of the neuropeptide during human pIN development. In addition, we hypothesize that some of the SST-negative cells could develop into PV-type INs, despite only rare detection of PV protein or PV-associated PNN component WFA. The ability to identify PV-type hMGE-pINs could be limited due to a number of factors: human neocortical PV expression is first detected post-natally and increases dramatically during early childhood until age 10[78,94]; and the protracted electrophysiological and neurochemical maturation is recapitulated in the rodent cortex and HC, where PV expression is first detected post-natally.[95] Similarly, analyses of human cortical and hippocampal samples demonstrated that PNNs, which regulate the fast-spiking properties of PV INs and are disrupted in epilepsy,[83,96] begin to form after birth and are not robustly expressed until the age of 8 years.[97] Furthermore, some fast-spiking cells do not contain detectable levels of PV protein or transcript, as has been documented for a substantial fraction of chandelier cells in the mouse cortex[98] and some basket and bistratified cells in the CA1 of the mouse HC.[77] Finally, based on profiling studies in mouse and human, a subset of MGE-pINs share characteristics of both PV and SST subtypes.[77,94,99] Nevertheless, human cells were of a definitive GABAergic MGE-pIN identity and sufficiently functional to eliminate mesiotemporal seizures in most of the cell-treated animals by 5–7 MPT, despite being electrophysiologically and neurochemically immature.

The mechanism of action of the grafted MGE-pINs in the epileptic HC, and whether it is linked specifically to synaptic GABAergic inhibition of host excitatory neurons, has not been elucidated here. Future experiments with optogenetically modified pINs or designer receptors exclusively activated by designer drugs (DREADDs) may help to inform a mechanism of action.

Overall, this study demonstrates significant preclinical efficacy and preliminary safety of a hESC-derived GABAergic MGE pallial-type IN cell therapy candidate, supporting further development of this approach for the potential future treatment of chronic focal epilepsy.

STAR★METHODS

Detailed methods are provided in the online version of this paper and include the following:

- KEY RESOURCES TABLE
- RESOURCE AVAILABILITY
  - Lead contact
  - Materials availability
  - Data and code availability
- EXPERIMENTAL MODEL AND STUDY PARTICIPANT DETAILS
  - Institutional oversight
  - hESC line and banks
  - hESC stability
  - Animals
- METHOD DETAILS
  - hESC expansion
  - MGE pallial-type interneuron differentiation
  - Cell batch processing and cryopreservation
  - Immunocytochemistry
  - Assessment of residual pluripotent cells by flow cytometry
  - Primeflow
  - GABA release
  - In vitro cell migration
  - Single cell RNA sequencing
  - Epilepsy induction
  - Cell transplantation into the MTLE mouse model
  - Electrode implantation and EEG recording
  - Criteria for exclusion
  - Brain slice electrophysiology
  - Behavior
  - Perfusion
  - EEG analysis
  - RNA FISH
  - Histology
  - Measurement of GC dispersion width and area
- QUANTIFICATION AND STATISTICAL ANALYSIS
  - Statistical analysis
  - Randomization and masking
- ADDITIONAL RESOURCES

at each time point are indicated by asterisk (*$p < 0.05$), Mann-Whitney test (200-K and 1.5-M dose groups vs. respective vehicle groups). Kruskal-Wallis test between 25-K and 50-K vs. corresponding vehicle group was not significant at any of the time points. A responder-rate threshold was designated for animals exhibiting >75% reduction vs. vehicle (depicted as red, dashed line).
(B–D) Histology panel shows human cell persistence (HNA+), distribution, and fate in the epileptic HC for the four doses at 8.5 MPT. (C and D) Higher magnification images of the corresponding dentate gyrus showing expression of MGE markers LHX6 (C) and SST (D). Scale bars are 500 μm (B) and 200 μm (C and D).
(E–J) Quantification of human cell persistence and fate of lots 2-U and 2-S. Total persisting human cell number marked by (E) HNA, (F) HNA/LHX6, and (G) HNA/SST at 8.5 MPT. (H) Relative human cell persistence as a percentage of HNA cells over the initial dose. (I and J) Quantification of LHX6 (I) and SST (J) out of the total persisting human cells (HNA+). All data are mean ± SEM.

CellPress
OPEN ACCESS

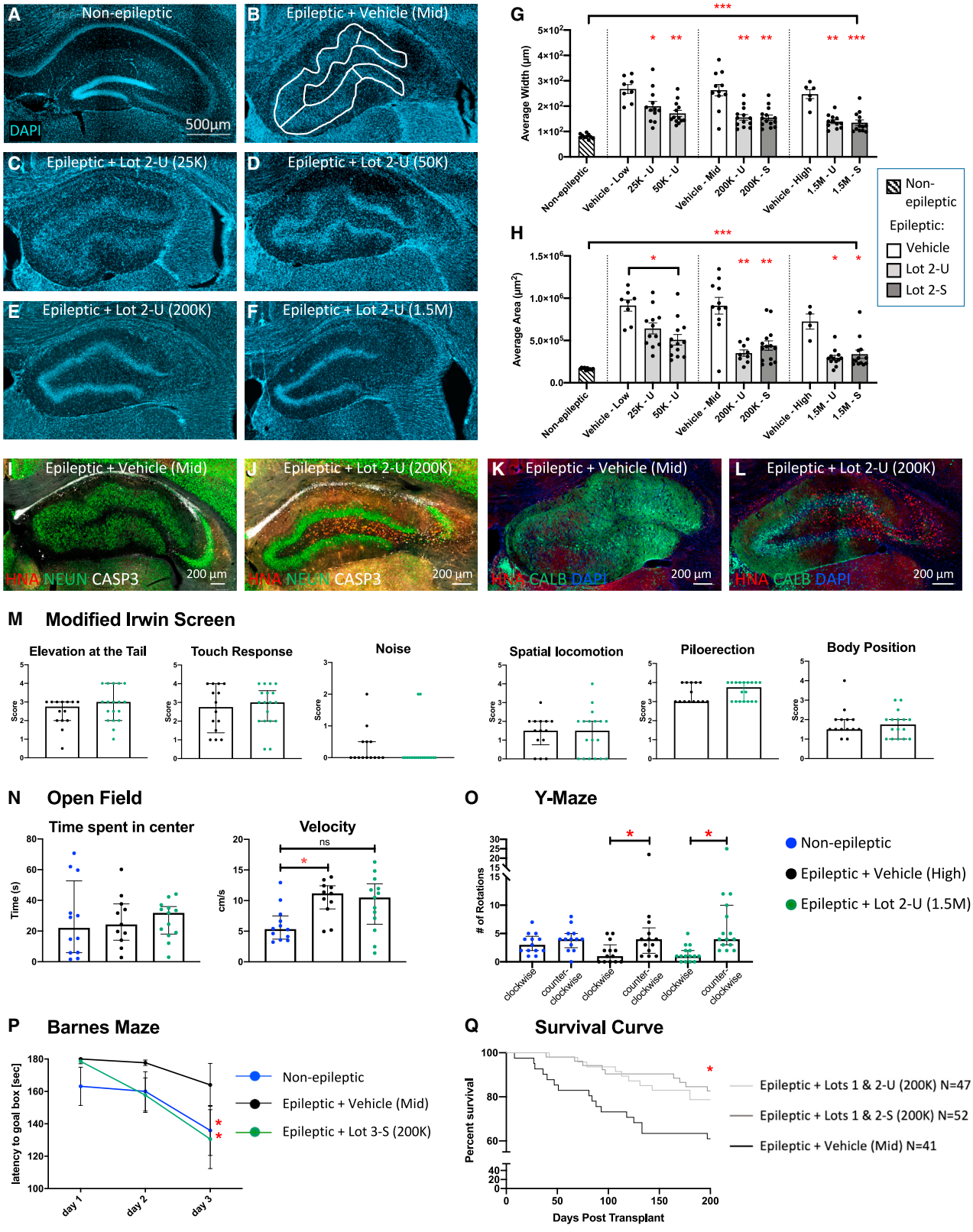

Figure 7. Epileptic HC pathology, behavioral outcome, and animal survival after human pIN transplantation

(A–H) Granule cell (GC) dispersion analysis at 8.5 MPT in age-matched mice: DAPI labeling shows representative GC layer in (A) naive mouse, (B) epileptic vehicle-treated mouse, and (C–F) epileptic cell-treated mice transplanted with 25-K, 50-K, 200-K, and 1.5-M human cells/HC of lot 2-U. Scale bar is 500 µm. (G and H)

(legend continued on next page)

SUPPLEMENTAL INFORMATION

Supplemental information can be found online at https://doi.org/10.1016/j.stem.2023.08.013.

ACKNOWLEDGMENTS

This work was supported by the California Institute for Regenerative Medicine (CIRM; grants: DISC-10525 and TRAN-11611) to the principal investigator, C.R.N. We thank Christopher Abilay, Srijana Balasundar, Daniel Cherkowsky, Mackenzie Englund, Margaret Cobos, Berenise De Haro, Brianna Feld, Jack Hardiman, Alicia Lee, Jennifer Leedy, Megan Masnaghetti, Alfredo Mejia, Seona Patel, Nafees Rahman, Alex Scibetta, Olga Sanchez, Anita Spasova, Alexandra Vogel, and Dosh Whye for their skillful technical contributions.

AUTHOR CONTRIBUTIONS

Conceptualization, M.B., S.B., M.P., Y.M., S.H., G.B., A.B., C.P., C.R.N., A.K., J.R., and A.A.-B.; investigation, M.B., S.B., M.P., Y.M., S.H., R.Z., S.L., M.W., P.H., H.K., W.B., E.S.S., D.T., G.S., M.S., N.S., A.N., H.N., W.A., S.K., L.F., J.S., and L.Z.; formal analysis, M.B., S.B., M.P., Y.M., S.H., R.Z., S.L., M.W., P.H., H.K., W.B., E.S.S., D.T., G.S., M.S., N.S., A.N., H.N., W.A., S.K., L.F., J.S., and L.Z.; writing – original draft, M.B., S.B., M.P., and C.R.N.; writing – review & editing, M.B., S.B., M.P., Y.M., S.H., A.B., C.P., and C.R.N.; supervision, G.B., A.B., C.P., and C.R.N.

DECLARATION OF INTERESTS

All authors except for L.Z. are employees and/or shareholders of Neurona Therapeutics Inc. C.R.N., J.R., A.K., and A.A.-B. are founders of Neurona. J.R., A.K., and A.A.-B. are members of the scientific advisory board at Neurona.

Received: July 9, 2022
Revised: March 17, 2023
Accepted: August 25, 2023
Published: October 5, 2023

REFERENCES

1. Fisher, R.S., van Emde Boas, W., Blume, W., Elger, C., Genton, P., Lee, P., and Engel, J., Jr. (2005). Epileptic seizures and epilepsy: definitions proposed by the International League Against Epilepsy (ILAE) and the International Bureau for Epilepsy (IBE). Epilepsia *46*, 470–472. https://doi.org/10.1111/j.0013-9580.2005.66104.x.
2. Walia, K.S., Khan, E.A., Ko, D.H., Raza, S.S., and Khan, Y.N. (2004). Side effects of antiepileptics–a review. Pain Pract. *4*, 194–203. https://doi.org/10.1111/j.1533-2500.2004.04304.x.
3. Cramer, J.A., Mintzer, S., Wheless, J., and Mattson, R.H. (2010). Adverse effects of antiepileptic drugs: a brief overview of important issues. Expert Rev. Neurother. *10*, 885–891. https://doi.org/10.1586/ern.10.71.
4. Leppik, I.E. (1992). Intractable epilepsy in adults. Epilepsy Res. Suppl. *5*, 7–11.
5. Schmidt, D., and Löscher, W. (2005). Drug resistance in epilepsy: putative neurobiologic and clinical mechanisms. Epilepsia *46*, 858–877. https://doi.org/10.1111/j.1528-1167.2005.54904.x.
6. Rogawski, M.A., and Holmes, G.L. (2009). Nontraditional epilepsy treatment approaches. Neurotherapeutics *6*, 213–217. https://doi.org/10.1016/j.nurt.2009.02.002.
7. Wiebe, S., Blume, W.T., Girvin, J.P., and Eliasziw, M.; Effectiveness and Efficiency of Surgery for Temporal Lobe Epilepsy Study Group (2001). A randomized, controlled trial of surgery for temporal-lobe epilepsy. N. Engl. J. Med. *345*, 311–318. https://doi.org/10.1056/NEJM200108023450501.
8. Pereira Dalio, M.T.R., Velasco, T.R., Feitosa, I.D.F., Assirati Junior, J.A., Carlotti Junior, C.G., Leite, J.P., Dos Santos, A.C., Alexandre, V., Nakano, F.N., Saute, R.L., et al. (2022). Long-term outcome of temporal lobe epilepsy surgery in 621 patients with hippocampal sclerosis: clinical and surgical prognostic factors. Front. Neurol. *13*, 833293. https://doi.org/10.3389/fneur.2022.833293.
9. Nilsen, K.E., and Cock, H.R. (2004). Focal treatment for refractory epilepsy: hope for the future? Brain Res. Brain Res. Rev. *44*, 141–153. https://doi.org/10.1016/j.brainresrev.2003.11.003.
10. Huang, Z.J. (2014). Toward a genetic dissection of cortical circuits in the mouse. Neuron *83*, 1284–1302. https://doi.org/10.1016/j.neuron.2014.08.041.
11. Hu, J.S., Vogt, D., Sandberg, M., and Rubenstein, J.L. (2017). Cortical interneuron development: a tale of time and space. Development *144*, 3867–3878. https://doi.org/10.1242/dev.132852.
12. Bandler, R.C., Mayer, C., and Fishell, G. (2017). Cortical interneuron specification: the juncture of genes, time and geometry. Curr. Opin. Neurobiol. *42*, 17–24. https://doi.org/10.1016/j.conb.2016.10.003.
13. Lim, L., Mi, D., Llorca, A., and Marín, O. (2018). Development and functional diversification of cortical interneurons. Neuron *100*, 294–313. https://doi.org/10.1016/j.neuron.2018.10.009.
14. Wonders, C.P., and Anderson, S.A. (2006). The origin and specification of cortical interneurons. Nat. Rev. Neurosci. *7*, 687–696. https://doi.org/10.1038/nrn1954.
15. Gelman, D., Griveau, A., Dehorter, N., Teissier, A., Varela, C., Pla, R., Pierani, A., and Marín, O. (2011). A wide diversity of cortical GABAergic interneurons derives from the embryonic preoptic area. J. Neurosci. *31*, 16570–16580. https://doi.org/10.1523/JNEUROSCI.4068-11.2011.
16. de Lanerolle, N.C., Kim, J.H., Robbins, R.J., and Spencer, D.D. (1989). Hippocampal interneuron loss and plasticity in human temporal lobe epilepsy. Brain Res. *495*, 387–395. https://doi.org/10.1016/0006-8993(89)90234-5.
17. de Lanerolle, N.C., Kim, J.H., Williamson, A., Spencer, S.S., Zaveri, H.P., Eid, T., and Spencer, D.D. (2003). A retrospective analysis of hippocampal pathology in human temporal lobe epilepsy: evidence for distinctive patient subcategories. Epilepsia *44*, 677–687. https://doi.org/10.1046/j.1528-1157.2003.32701.x.
18. Arellano, J.I., Muñoz, A., Ballesteros-Yáñez, I., Sola, R.G., and DeFelipe, J. (2004). Histopathology and reorganization of chandelier cells in the

Average GC layer width (G) was measured at three places, as illustrated with white lines in (B), and GC layer area (H) was measured as illustrated with a white boundary in (B). Three vehicle groups were used to match the delivery volumes of the respective cell doses, labeled as Vehicle-Low, Vehicle-Mid, and Vehicle-High. The Kruskal-Wallis statistic, followed by Dunn's test, was significant between cell and vehicle groups at all doses for both unsorted and sorted lots ($p < 0.05$).
(I and J) Apoptotic cell labeling with cleaved CASP3 in (I) vehicle- or (J) cell-treated mice.
(K and L) IHC staining for endogenous CALB-expressing neurons in the GC layer of (K) vehicle- or (L) cell-treated mice. Scale bars are 200 μm (I–L).
(M–O) Data are shown for the highest tested dose of 1.5-M cells/HC of lot 2-U (green). All data are expressed as median with interquartile range. (M) Modified Irwin screen (sedation). (N) Open-field test (general anxiety, spatial locomotion, and travel velocity). (O) Y-maze test (spatial memory).
(P) Barnes maze (learning and memory) using naive mice (blue, n = 13), epileptic vehicle-injected mice (black, n = 11), and epileptic cell-transplanted mice with 200-K cell dose (green, n = 13). Mann-Whitney test for differences between cell and vehicle groups; significant differences are indicated by asterisk (*$p < 0.05$).
(Q) Survival curves for epileptic animals treated with either vehicle (black) or transplanted with unsorted (200-K, lots 1-U/2-U, light gray, n = 47) or sorted (200-K, lots 1-S/2-S dark gray, n = 52). Significantly increased survival at 200 days post-transplant was observed with both unsorted and sorted cell lots compared with vehicle treatment (chi-squared test, *$p < 0.05$).
All data are mean ± SEM.

human epileptic sclerotic hippocampus. Brain *127*, 45–64. https://doi.org/10.1093/brain/awh004.

19. Andrioli, A., Alonso-Nanclares, L., Arellano, J.I., and DeFelipe, J. (2007). Quantitative analysis of parvalbumin-immunoreactive cells in the human epileptic hippocampus. Neuroscience *149*, 131–143. https://doi.org/10.1016/j.neuroscience.2007.07.029.
20. Rossignol, E. (2011). Genetics and function of neocortical GABAergic interneurons in neurodevelopmental disorders. Neural Plast. *2011*, 649325. https://doi.org/10.1155/2011/649325.
21. Anwar, A., Saleem, S., Patel, U.K., Arumaithurai, K., and Malik, P. (2019). Dravet syndrome: an overview. Cureus *11*, e5006. https://doi.org/10.7759/cureus.5006.
22. Cobos, I., Calcagnotto, M.E., Vilaythong, A.J., Thwin, M.T., Noebels, J.L., Baraban, S.C., and Rubenstein, J.L. (2005). Mice lacking Dlx1 show subtype-specific loss of interneurons, reduced inhibition and epilepsy. Nat. Neurosci. *8*, 1059–1068. https://doi.org/10.1038/nn1499.
23. Kobayashi, M., and Buckmaster, P.S. (2003). Reduced inhibition of dentate granule cells in a model of temporal lobe epilepsy. J. Neurosci. *23*, 2440–2452. https://doi.org/10.1523/JNEUROSCI.23-06-02440.2003.
24. Peng, Z., Zhang, N., Wei, W., Huang, C.S., Cetina, Y., Otis, T.S., and Houser, C.R. (2013). A reorganized GABAergic circuit in a model of epilepsy: evidence from optogenetic labeling and stimulation of somatostatin interneurons. J. Neurosci. *33*, 14392–14405. https://doi.org/10.1523/JNEUROSCI.2045-13.2013.
25. Krook-Magnuson, E., Armstrong, C., Oijala, M., and Soltesz, I. (2013). On-demand optogenetic control of spontaneous seizures in temporal lobe epilepsy. Nat. Commun. *4*, 1376. https://doi.org/10.1038/ncomms2376.
26. Hofmann, G., Balgooyen, L., Mattis, J., Deisseroth, K., and Buckmaster, P.S. (2016). Hilar somatostatin interneuron loss reduces dentate gyrus inhibition in a mouse model of temporal lobe epilepsy. Epilepsia *57*, 977–983. https://doi.org/10.1111/epi.13376.
27. Wichterle, H., Garcia-Verdugo, J.M., Herrera, D.G., and Alvarez-Buylla, A. (1999). Young neurons from medial ganglionic eminence disperse in adult and embryonic brain. Nat. Neurosci. *2*, 461–466.
28. Alvarez-Dolado, M., Calcagnotto, M.E., Karkar, K.M., Southwell, D.G., Jones-Davis, D.M., Estrada, R.C., Rubenstein, J.L., Alvarez-Buylla, A., and Baraban, S.C. (2006). Cortical inhibition modified by embryonic neural precursors grafted into the postnatal brain. J. Neurosci. *26*, 7380–7389. https://doi.org/10.1523/JNEUROSCI.1540-06.2006.
29. Baraban, S.C., Southwell, D.G., Estrada, R.C., Jones, D.L., Sebe, J.Y., Alfaro-Cervello, C., García-Verdugo, J.M., Rubenstein, J.L., and Alvarez-Buylla, A. (2009). Reduction of seizures by transplantation of cortical GABAergic interneuron precursors into Kv1.1 mutant mice. Proc. Natl. Acad. Sci. USA *106*, 15472–15477. https://doi.org/10.1073/pnas.0900141106.
30. Waldau, B., Hattiangady, B., Kuruba, R., and Shetty, A.K. (2010). Medial ganglionic eminence-derived neural stem cell grafts ease spontaneous seizures and restore GDNF expression in a rat model of chronic temporal lobe epilepsy. Stem Cells *28*, 1153–1164. https://doi.org/10.1002/stem.446.
31. Calcagnotto, M.E., Ruiz, L.P., Blanco, M.M., Santos-Junior, J.G., Valente, M.F., Patti, C., Frussa-Filho, R., Santiago, M.F., Zipancic, I., Alvarez-Dolado, M., et al. (2010). Effect of neuronal precursor cells derived from medial ganglionic eminence in an acute epileptic seizure model. Epilepsia *51*, 71–75. https://doi.org/10.1111/j.1528-1167.2010.02614.x.
32. Hunt, R.F., Girskis, K.M., Rubenstein, J.L., Alvarez-Buylla, A., and Baraban, S.C. (2013). GABA progenitors grafted into the adult epileptic brain control seizures and abnormal behavior. Nat. Neurosci. *16*, 692–697. https://doi.org/10.1038/nn.3392.
33. Henderson, K.W., Gupta, J., Tagliatela, S., Litvina, E., Zheng, X., Van Zandt, M.A., Woods, N., Grund, E., Lin, D., Royston, S., et al. (2014). Long-term seizure suppression and optogenetic analyses of synaptic connectivity in epileptic mice with hippocampal grafts of GABAergic interneurons. J. Neurosci. *34*, 13492–13504. https://doi.org/10.1523/JNEUROSCI.0005-14.2014.
34. Romariz, S.A., Paiva, D.S., Galindo, L.T., Barnabé, G.F., Guedes, V.A., Borlongan, C.V., and Longo, B.M. (2017). Medial ganglionic eminence cells freshly obtained or expanded as neurospheres show distinct cellular and molecular properties in reducing epileptic seizures. CNS Neurosci. Ther. *23*, 127–134. https://doi.org/10.1111/cns.12650.
35. Howard, M.A., Rubenstein, J.L., and Baraban, S.C. (2014). Bidirectional homeostatic plasticity induced by interneuron cell death and transplantation in vivo. Proc. Natl. Acad. Sci. USA *111*, 492–497. https://doi.org/10.1073/pnas.1307784111.
36. Casalia, M.L., Howard, M.A., and Baraban, S.C. (2017). Persistent seizure control in epileptic mice transplanted with gamma-aminobutyric acid progenitors. Ann. Neurol. *82*, 530–542. https://doi.org/10.1002/ana.25021.
37. Nicholas, C.R., Chen, J., Tang, Y., Southwell, D.G., Chalmers, N., Vogt, D., Arnold, C.M., Chen, Y.J., Stanley, E.G., Elefanty, A.G., et al. (2013). Functional maturation of hPSC-derived forebrain interneurons requires an extended timeline and mimics human neural development. Cell Stem Cell *12*, 573–586. https://doi.org/10.1016/j.stem.2013.04.005.
38. Maroof, A.M., Keros, S., Tyson, J.A., Ying, S.W., Ganat, Y.M., Merkle, F.T., Liu, B., Goulburn, A., Stanley, E.G., Elefanty, A.G., et al. (2013). Directed differentiation and functional maturation of cortical interneurons from human embryonic stem cells. Cell Stem Cell *12*, 559–572. https://doi.org/10.1016/j.stem.2013.04.008.
39. Liu, Y., Weick, J.P., Liu, H., Krencik, R., Zhang, X., Ma, L., Zhou, G.M., Ayala, M., and Zhang, S.C. (2013). Medial ganglionic eminence-like cells derived from human embryonic stem cells correct learning and memory deficits. Nat. Biotechnol. *31*, 440–447. https://doi.org/10.1038/nbt.2565.
40. Kim, T.G., Yao, R., Monnell, T., Cho, J.H., Vasudevan, A., Koh, A., Peeyush, K.T., Moon, M., Datta, D., Bolshakov, V.Y., et al. (2014). Efficient specification of interneurons from human pluripotent stem cells by dorsoventral and rostrocaudal modulation. Stem Cells *32*, 1789–1804. https://doi.org/10.1002/stem.1704.
41. Meganathan, K., Lewis, E.M.A., Gontarz, P., Liu, S., Stanley, E.G., Elefanty, A.G., Huettner, J.E., Zhang, B., and Kroll, K.L. (2017). Regulatory networks specifying cortical interneurons from human embryonic stem cells reveal roles for CHD2 in interneuron development. Proc. Natl. Acad. Sci. USA *114*, E11180–E11189. https://doi.org/10.1073/pnas.1712365115.
42. Close, J.L., Yao, Z., Levi, B.P., Miller, J.A., Bakken, T.E., Menon, V., Ting, J.T., Wall, A., Krostag, A.R., Thomsen, E.R., et al. (2017). Single-cell profiling of an in vitro model of human interneuron development reveals temporal dynamics of cell type production and maturation. Neuron *93*, 1035–1048.e5. https://doi.org/10.1016/j.neuron.2017.02.014.
43. Wang, C., Najm, R., Xu, Q., Jeong, D.E., Walker, D., Balestra, M.E., Yoon, S.Y., Yuan, H., Li, G., Miller, Z.A., et al. (2018). Gain of toxic apolipoprotein E4 effects in human iPSC-derived neurons is ameliorated by a small-molecule structure corrector. Nat. Med. *24*, 647–657. https://doi.org/10.1038/s41591-018-0004-z.
44. Ni, P., Noh, H., Shao, Z., Zhu, Q., Guan, Y., Park, J.J., Arif, F., Park, J.M., Abani, C., Beaudreault, C., et al. (2019). Large-scale generation and characterization of homogeneous populations of migratory cortical interneurons from human pluripotent stem cells. Mol. Ther. Methods Clin. Dev. *13*, 414–430. https://doi.org/10.1016/j.omtm.2019.04.002.
45. Cunningham, M., Cho, J.H., Leung, A., Savvidis, G., Ahn, S., Moon, M., Lee, P.K., Han, J.J., Azimi, N., Kim, K.S., et al. (2014). hPSC-derived maturing GABAergic interneurons ameliorate seizures and abnormal behavior in epileptic mice. Cell Stem Cell *15*, 559–573. https://doi.org/10.1016/j.stem.2014.10.006.
46. Upadhya, D., Hattiangady, B., Castro, O.W., Shuai, B., Kodali, M., Attaluri, S., Bates, A., Dong, Y., Zhang, S.C., Prockop, D.J., and Shetty, A.K. (2019). Human induced pluripotent stem cell-derived MGE cell grafting after status epilepticus attenuates chronic epilepsy and

comorbidities via synaptic integration. Proc. Natl. Acad. Sci. USA *116*, 287–296. https://doi.org/10.1073/pnas.1814185115.

47. Waloschková, E., Gonzalez-Ramos, A., Mikroulis, A., Kudláček, J., Andersson, M., Ledri, M., and Kokaia, M. (2021). Human stem cell-derived GABAergic interneurons establish efferent synapses onto host neurons in rat epileptic hippocampus and inhibit spontaneous recurrent seizures. Int. J. Mol. Sci. *22*, 13243. https://doi.org/10.3390/ijms222413243.
48. Zhu, Q., Mishra, A., Park, J.S., Liu, D., Le, D.T., Gonzalez, S.Z., Anderson-Crannage, M., Park, J.M., Park, G.H., Tarbay, L., et al. (2023). Human cortical interneurons optimized for grafting specifically integrate, abort seizures, and display prolonged efficacy without over-inhibition. Neuron *111*, 807–823.e7. https://doi.org/10.1016/j.neuron.2022.12.014.
49. Xu, Q., Tam, M., and Anderson, S.A. (2008). Fate mapping Nkx2.1-lineage cells in the mouse telencephalon. J. Comp. Neurol. *506*, 16–29. https://doi.org/10.1002/cne.21529.
50. Fragkouli, A., van Wijk, N.V., Lopes, R., Kessaris, N., and Pachnis, V. (2009). LIM homeodomain transcription factor-dependent specification of bipotential MGE progenitors into cholinergic and GABAergic striatal interneurons. Development *136*, 3841–3851. https://doi.org/10.1242/dev.038083.
51. Flandin, P., Kimura, S., and Rubenstein, J.L. (2010). The progenitor zone of the ventral medial ganglionic eminence requires Nkx2-1 to generate most of the globus pallidus but few neocortical interneurons. J. Neurosci. *30*, 2812–2823. https://doi.org/10.1523/JNEUROSCI.4228-09.2010.
52. Nóbrega-Pereira, S., Gelman, D., Bartolini, G., Pla, R., Pierani, A., and Marín, O. (2010). Origin and molecular specification of globus pallidus neurons. J. Neurosci. *30*, 2824–2834. https://doi.org/10.1523/JNEUROSCI.4023-09.2010.
53. Marín, O., and Rubenstein, J.L. (2003). Cell migration in the forebrain. Annu. Rev. Neurosci. *26*, 441–483. https://doi.org/10.1146/annurev.neuro.26.041002.131058.
54. Su-Feher, L., Rubin, A.N., Silberberg, S.N., Catta-Preta, R., Lim, K.J., Ypsilanti, A.R., Zdilar, I., McGinnis, C.S., McKinsey, G.L., Rubino, T.E., Jr., et al. (2022). Single cell enhancer activity distinguishes GABAergic and cholinergic lineages in embryonic mouse basal ganglia. Proc. Natl. Acad. Sci. USA *119*, e2108760119. https://doi.org/10.1073/pnas.2108760119.
55. Kessaris, N., Fogarty, M., Iannarelli, P., Grist, M., Wegner, M., and Richardson, W.D. (2006). Competing waves of oligodendrocytes in the forebrain and postnatal elimination of an embryonic lineage. Nat. Neurosci. *9*, 173–179. https://doi.org/10.1038/nn1620.
56. Minocha, S., Valloton, D., Ypsilanti, A.R., Fiumelli, H., Allen, E.A., Yanagawa, Y., Marin, O., Chédotal, A., Hornung, J.P., and Lebrand, C. (2015). Nkx2.1-derived astrocytes and neurons together with Slit2 are indispensable for anterior commissure formation. Nat Commun *6*, 6887. https://doi.org/10.1038/ncomms7887.
57. Sussel, L., Marin, O., Kimura, S., and Rubenstein, J.L. (1999). Loss of Nkx2.1 homeobox gene function results in a ventral to dorsal molecular respecification within the basal telencephalon: evidence for a transformation of the pallidum into the striatum. Development *126*, 3359–3370. https://doi.org/10.1242/dev.126.15.3359.
58. Fogarty, M., Grist, M., Gelman, D., Marín, O., Pachnis, V., and Kessaris, N. (2007). Spatial genetic patterning of the embryonic neuroepithelium generates GABAergic interneuron diversity in the adult cortex. J. Neurosci. *27*, 10935–10946. https://doi.org/10.1523/JNEUROSCI.1629-07.2007.
59. Liodis, P., Denaxa, M., Grigoriou, M., Akufo-Addo, C., Yanagawa, Y., and Pachnis, V. (2007). Lhx6 activity is required for the normal migration and specification of cortical interneuron subtypes. J. Neurosci. *27*, 3078–3089. https://doi.org/10.1523/JNEUROSCI.3055-06.2007.
60. Zhao, Y., Flandin, P., Long, J.E., Cuesta, M.D., Westphal, H., and Rubenstein, J.L. (2008). Distinct molecular pathways for development of telencephalic interneuron subtypes revealed through analysis of Lhx6 mutants. J. Comp. Neurol. *510*, 79–99. https://doi.org/10.1002/cne.21772.
61. Zeisel, A., Muñoz-Manchado, A.B., Codeluppi, S., Lönnerberg, P., La Manno, G., Juréus, A., Marques, S., Munguba, H., He, L., Betsholtz, C., et al. (2015). Brain structure. Cell types in the mouse cortex and hippocampus revealed by single-cell RNA-seq. Science *347*, 1138–1142. https://doi.org/10.1126/science.aaa1934.
62. Paul, A., Crow, M., Raudales, R., He, M., Gillis, J., and Huang, Z.J. (2017). Transcriptional architecture of synaptic communication delineates GABAergic neuron identity. Cell *171*, 522–539.e20. https://doi.org/10.1016/j.cell.2017.08.032.
63. Yau, H.J., Wang, H.F., Lai, C., and Liu, F.C. (2003). Neural development of the neuregulin receptor ErbB4 in the cerebral cortex and the hippocampus: preferential expression by interneurons tangentially migrating from the ganglionic eminences. Cereb. Cortex *13*, 252–264. https://doi.org/10.1093/cercor/13.3.252.
64. Flames, N., Long, J.E., Garratt, A.N., Fischer, T.M., Gassmann, M., Birchmeier, C., Lai, C., Rubenstein, J.L., and Marín, O. (2004). Short- and long-range attraction of cortical GABAergic interneurons by neuregulin-1. Neuron *44*, 251–261. https://doi.org/10.1016/j.neuron.2004.09.028.
65. Cobos, I., Long, J.E., Thwin, M.T., and Rubenstein, J.L. (2006). Cellular patterns of transcription factor expression in developing cortical interneurons. Cereb. Cortex *16*, i82–i88. https://doi.org/10.1093/cercor/bhk003.
66. McKinsey, G.L., Lindtner, S., Trzcinski, B., Visel, A., Pennacchio, L.A., Huylebroeck, D., Higashi, Y., and Rubenstein, J.L. (2013). Dlx1&2-dependent expression of Zfhx1b (Sip1, Zeb2) regulates the fate switch between cortical and striatal interneurons. Neuron *77*, 83–98. https://doi.org/10.1016/j.neuron.2012.11.035.
67. Pai, E.L., Vogt, D., Clemente-Perez, A., McKinsey, G.L., Cho, F.S., Hu, J.S., Wimer, M., Paul, A., Fazel Darbandi, S., Pla, R., et al. (2019). Mafb and c-Maf have prenatal compensatory and postnatal antagonistic roles in cortical interneuron fate and function. Cell Rep. *26*, 1157–1173.e5. https://doi.org/10.1016/j.celrep.2019.01.031.
68. Pai, E.L., Chen, J., Fazel Darbandi, S., Cho, F.S., Chen, J., Lindtner, S., Chu, J.S., Paz, J.T., Vogt, D., Paredes, M.F., and Rubenstein, J.L. (2020). Maf and Mafb control mouse pallial interneuron fate and maturation through neuropsychiatric disease gene regulation. Elife *9*, e54903. https://doi.org/10.7554/eLife.54903.
69. Chen, Y.J., Friedman, B.A., Ha, C., Durinck, S., Liu, J., Rubenstein, J.L., Seshagiri, S., and Modrusan, Z. (2017). Single-cell RNA sequencing identifies distinct mouse medial ganglionic eminence cell types. Sci. Rep. *7*, 45656. https://doi.org/10.1038/srep45656.
70. Shi, Y., Wang, M., Mi, D., Lu, T., Wang, B., Dong, H., Zhong, S., Chen, Y., Sun, L., Zhou, X., et al. (2021). Mouse and human share conserved transcriptional programs for interneuron development. Science *374*, eabj6641. https://doi.org/10.1126/science.abj6641.
71. Tiklová, K., Nolbrant, S., Fiorenzano, A., Björklund, Å.K., Sharma, Y., Heuer, A., Gillberg, L., Hoban, D.B., Cardoso, T., Adler, A.F., et al. (2020). Single cell transcriptomics identifies stem cell-derived graft composition in a model of Parkinson's disease. Nat. Commun. *11*, 2434. https://doi.org/10.1038/s41467-020-16225-5.
72. Feng, J., Bi, C., Clark, B.S., Mady, R., Shah, P., and Kohtz, J.D. (2006). The Evf-2 noncoding RNA is transcribed from the Dlx-5/6 ultraconserved region and functions as a Dlx-2 transcriptional coactivator. Genes Dev. *20*, 1470–1484. https://doi.org/10.1101/gad.1416106.
73. Chen, L., Chatterjee, M., and Li, J.Y. (2010). The mouse homeobox gene Gbx2 is required for the development of cholinergic interneurons in the striatum. J. Neurosci. *30*, 14824–14834. https://doi.org/10.1523/JNEUROSCI.3742-10.2010.
74. Mayer, C., Hafemeister, C., Bandler, R.C., Machold, R., Batista Brito, R., Jaglin, X., Allaway, K., Butler, A., Fishell, G., and Satija, R. (2018).

Developmental diversification of cortical inhibitory interneurons. Nature *555*, 457–462. https://doi.org/10.1038/nature25999.

75. Batista-Brito, R., Machold, R., Klein, C., and Fishell, G. (2008). Gene expression in cortical interneuron precursors is prescient of their mature function. Cereb. Cortex *18*, 2306–2317. https://doi.org/10.1093/cercor/bhm258.
76. Tasic, B., Menon, V., Nguyen, T.N., Kim, T.K., Jarsky, T., Yao, Z., Levi, B., Gray, L.T., Sorensen, S.A., Dolbeare, T., et al. (2016). Adult mouse cortical cell taxonomy revealed by single cell transcriptomics. Nat. Neurosci. *19*, 335–346. https://doi.org/10.1038/nn.4216.
77. Harris, K.D., Hochgerner, H., Skene, N.G., Magno, L., Katona, L., Bengtsson Gonzales, C., Somogyi, P., Kessaris, N., Linnarsson, S., and Hjerling-Leffler, J. (2018). Classes and continua of hippocampal CA1 inhibitory neurons revealed by single-cell transcriptomics. PLoS Biol. *16*, e2006387. https://doi.org/10.1371/journal.pbio.2006387.
78. Fung, S.J., Webster, M.J., Sivagnanasundaram, S., Duncan, C., Elashoff, M., and Weickert, C.S. (2010). Expression of interneuron markers in the dorsolateral prefrontal cortex of the developing human and in schizophrenia. Am. J. Psychiatry *167*, 1479–1488. https://doi.org/10.1176/appi.ajp.2010.09060784.
79. Riban, V., Bouilleret, V., Pham-Lê, B.T., Fritschy, J.M., Marescaux, C., and Depaulis, A. (2002). Evolution of hippocampal epileptic activity during the development of hippocampal sclerosis in a mouse model of temporal lobe epilepsy. Neuroscience *112*, 101–111. https://doi.org/10.1016/s0306-4522(02)00064-7.
80. Gouder, N., Fritschy, J.M., and Boison, D. (2003). Seizure suppression by adenosine A1 receptor activation in a mouse model of pharmacoresistant epilepsy. Epilepsia *44*, 877–885. https://doi.org/10.1046/j.1528-1157.2003.03603.x.
81. Klein, S., Bankstahl, M., and Löscher, W. (2015). Inter-individual variation in the effect of antiepileptic drugs in the intrahippocampal kainate model of mesial temporal lobe epilepsy in mice. Neuropharmacology *90*, 53–62. https://doi.org/10.1016/j.neuropharm.2014.11.008.
82. Duveau, V., Pouyatos, B., Bressand, K., Bouyssières, C., Chabrol, T., Roche, Y., Depaulis, A., and Roucard, C. (2016). Differential effects of antiepileptic drugs on focal seizures in the intrahippocampal kainate mouse model of mesial temporal lobe epilepsy. CNS Neurosci. Ther. *22*, 497–506. https://doi.org/10.1111/cns.12523.
83. Chaunsali, L., Tewari, B.P., and Sontheimer, H. (2021). Perineuronal net dynamics in the pathophysiology of epilepsy. Epilepsy Curr. *21*, 273–281. https://doi.org/10.1177/15357597211018688.
84. Bouilleret, V., Ridoux, V., Depaulis, A., Marescaux, C., Nehlig, A., and Le Gal La Salle, G. (1999). Recurrent seizures and hippocampal sclerosis following intrahippocampal kainate injection in adult mice: electroencephalography, histopathology and synaptic reorganization similar to mesial temporal lobe epilepsy. Neuroscience *89*, 717–729. https://doi.org/10.1016/s0306-4522(98)00401-1.
85. Rougier, A., Arthaud, S., Zombre, N., and La Salle, G. (2005). Patterns of dentate granule cell responses to perforant path stimulation in epileptic mice with granule cell dispersion. Epilepsy Res. *63*, 119–129. https://doi.org/10.1016/j.eplepsyres.2005.01.004.
86. Blümcke, I., Spreafico, R., Haaker, G., Coras, R., Kobow, K., Bien, C.G., Pfäfflin, M., Elger, C., Widman, G., Schramm, J., et al. (2017). Histopathological findings in brain tissue obtained during epilepsy surgery. N. Engl. J. Med. *377*, 1648–1656. https://doi.org/10.1056/NEJMoa1703784.
87. Kiasalari, Z., Khalili, M., Shafiee, S., and Roghani, M. (2016). The effect of vitamin E on learning and memory deficits in intrahippocampal kainate-induced temporal lobe epilepsy in rats. Indian J. Pharmacol. *48*, 11–14. https://doi.org/10.4103/0253-7613.174394.
88. Abrous, D.N., Rodriguez, J.J., Montaron, M.F., Aurousseau, C., Le Moal, M., and Barneoud, P. (1998). Behavioural recovery after unilateral lesion of the dopaminergic mesotelencephalic pathway: effect of repeated testing. Neuroscience *84*, 213–221. https://doi.org/10.1016/s0306-4522(97)00498-3.
89. Levine, A.T., Born, H.A., Landstrom, A.P., Larson, S., Lee, W.L., Dao, A.T., Wehrens, X.H., Lai, Y.C., and Anderson, A.E. (2020). Cardiac dysregulation following intrahippocampal kainate-induced status epilepticus. Sci. Rep. *10*, 4043. https://doi.org/10.1038/s41598-020-60324-8.
90. Winawer, M.R., Makarenko, N., McCloskey, D.P., Hintz, T.M., Nair, N., Palmer, A.A., and Scharfman, H.E. (2007). Acute and chronic responses to the convulsant pilocarpine in DBA/2J and A/J mice. Neuroscience *149*, 465–475. https://doi.org/10.1016/j.neuroscience.2007.06.009.
91. Singh, A., and Trevick, S. (2016). The epidemiology of global epilepsy. Neurol. Clin. *34*, 837–847. https://doi.org/10.1016/j.ncl.2016.06.015.
92. Barker-Haliski, M.L., Johnson, K., Billingsley, P., Huff, J., Handy, L.J., Khaleel, R., Lu, Z., Mau, M.J., Pruess, T.H., Rueda, C., et al. (2017). Validation of a preclinical drug screening platform for pharmacoresistant epilepsy. Neurochem. Res. *42*, 1904–1918. https://doi.org/10.1007/s11064-017-2227-7.
93. Venceslas, D., and Corinne, R. (2017). A mesiotemporal lobe epilepsy mouse model. Neurochem. Res. *42*, 1919–1925. https://doi.org/10.1007/s11064-017-2239-3.
94. Herring, C.A., Simmons, R.K., Freytag, S., Poppe, D., Moffet, J.J.D., Pflueger, J., Buckberry, S., Vargas-Landin, D.B., Clément, O., Echeverría, E.G., et al. (2022). Human prefrontal cortex gene regulatory dynamics from gestation to adulthood at single-cell resolution. Cell *185*, 4428–4447.e28. https://doi.org/10.1016/j.cell.2022.09.039.
95. Solbach, S., and Celio, M.R. (1991). Ontogeny of the calcium binding protein parvalbumin in the rat nervous system. Anat. Embryol. (Berl.) *184*, 103–124. https://doi.org/10.1007/BF00942742.
96. Tewari, B.P., Chaunsali, L., Campbell, S.L., Patel, D.C., Goode, A.E., and Sontheimer, H. (2018). Perineuronal nets decrease membrane capacitance of peritumoral fast spiking interneurons in a model of epilepsy. Nat. Commun. *9*, 4724. https://doi.org/10.1038/s41467-018-07113-0.
97. Rogers, S.L., Rankin-Gee, E., Risbud, R.M., Porter, B.E., and Marsh, E.D. (2018). Normal development of the perineuronal net in humans; in patients with and without epilepsy. Neuroscience *384*, 350–360. https://doi.org/10.1016/j.neuroscience.2018.05.039.
98. Taniguchi, H., Lu, J., and Huang, Z.J. (2013). The spatial and temporal origin of chandelier cells in mouse neocortex. Science *339*, 70–74. https://doi.org/10.1126/science.1227622.
99. Bakken, T.E., Jorstad, N.L., Hu, Q., Lake, B.B., Tian, W., Kalmbach, B.E., Crow, M., Hodge, R.D., Krienen, F.M., Sorensen, S.A., et al. (2021). Comparative cellular analysis of motor cortex in human, marmoset and mouse. Nature *598*, 111–119. https://doi.org/10.1038/s41586-021-03465-8.
100. Lois, C., Hong, E.J., Pease, S., Brown, E.J., and Baltimore, D. (2002). Germline transmission and tissue-specific expression of transgenes delivered by lentiviral vectors. Science *295*, 868–872. https://doi.org/10.1126/science.1067081.
101. Zhang, F., Wang, L.P., Brauner, M., Liewald, J.F., Kay, K., Watzke, N., Wood, P.G., Bamberg, E., Nagel, G., Gottschalk, A., and Deisseroth, K. (2007). Multimodal fast optical interrogation of neural circuitry. Nature *446*, 633–639. https://doi.org/10.1038/nature05744.
102. Stuart, T., Butler, A., Hoffman, P., Hafemeister, C., Papalexi, E., Mauck, W. M., 3rd, Hao, Y., Stoeckius, M., Smibert, P., and Satija, R. (2019). Comprehensive Integration of Single-Cell Data. *Cell*, *177*, 1888–1902.e21. https://doi.org/10.1016/j.cell.2019.05.031.
103. Merkle, F.T., Ghosh, S., Kamitaki, N., Mitchell, J., Avior, Y., Mello, C., Kashin, S., Mekhoubad, S., Ilic, D., Charlton, M., et al. (2017). Human pluripotent stem cells recurrently acquire and expand dominant negative P53 mutations. Nature *545*, 229–233. https://doi.org/10.1038/nature22312.
104. Kilkenny, C., Browne, W.J., Cuthill, I.C., Emerson, M., and Altman, D.G. (2010). Improving bioscience research reporting: the ARRIVE guidelines for reporting animal research. PLoS Biol. *8*, e1000412. https://doi.org/10.1371/journal.pbio.1000412.

105. Twele, F., Töllner, K., Brandt, C., and Löscher, W. (2016). Significant effects of sex, strain, and anesthesia in the intrahippocampal kainate mouse model of mesial temporal lobe epilepsy. Epilepsy Behav. *55*, 47–56. https://doi.org/10.1016/j.yebeh.2015.11.027.

106. Ahn, S., Kim, T.G., Kim, K.S., and Chung, S. (2016). Differentiation of human pluripotent stem cells into Medial ganglionic Eminence vs. caudal ganglionic Eminence cells. Methods *101*, 103–112. https://doi.org/10.1016/j.ymeth.2015.09.009.

107. Nicoleau, C., Varela, C., Bonnefond, C., Maury, Y., Bugi, A., Aubry, L., Viegas, P., Bourgois-Rocha, F., Peschanski, M., and Perrier, A.L. (2013). Embryonic stem cells neural differentiation qualifies the role of Wnt/β-catenin signals in human telencephalic specification and regionalization. Stem Cells *31*, 1763–1774. https://doi.org/10.1002/stem.1462.

108. Qi, Y., Zhang, X.J., Renier, N., Wu, Z., Atkin, T., Sun, Z., Ozair, M.Z., Tchieu, J., Zimmer, B., Fattahi, F., et al. (2017). Combined small-molecule inhibition accelerates the derivation of functional cortical neurons from human pluripotent stem cells. Nat. Biotechnol. *35*, 154–163. https://doi.org/10.1038/nbt.3777.

109. Telezhkin, V., Schnell, C., Yarova, P., Yung, S., Cope, E., Hughes, A., Thompson, B.A., Sanders, P., Geater, C., Hancock, J.M., et al. (2016). Forced cell cycle exit and modulation of GABAA, CREB, and GSK3β signaling promote functional maturation of induced pluripotent stem cell-derived neurons. Am. J. Physiol. Cell Physiol. *310*, C520–C541. https://doi.org/10.1152/ajpcell.00166.2015.

110. Schidlitzki, A., Twele, F., Klee, R., Waltl, I., Römermann, K., Bröer, S., Meller, S., Gerhauser, I., Rankovic, V., Li, D., et al. (2017). A combination of NMDA and AMPA receptor antagonists retards granule cell dispersion and epileptogenesis in a model of acquired epilepsy. Sci. Rep. *7*, 12191. https://doi.org/10.1038/s41598-017-12368-6.

111. Ting, J.T., Lee, B.R., Chong, P., Soler-Llavina, G., Cobbs, C., Koch, C., Zeng, H., and Lein, E. (2018). Preparation of acute brain slices using an optimized N-methyl-D-glucamine protective recovery method. J. Vis. Exp.53825. https://doi.org/10.3791/53825.

112. Klee, R., Töllner, K., Rankovic, V., Römermann, K., Schidlitzki, A., Bankstahl, M., and Löscher, W. (2015). Network pharmacology for antiepileptogenesis: tolerability of multitargeted drug combinations in nonepileptic vs. post-status epilepticus mice. Epilepsy Res. *118*, 34–48. https://doi.org/10.1016/j.eplepsyres.2015.11.003.

113. Van Den Herrewegen, Y., Denewet, L., Buckinx, A., Albertini, G., Van Eeckhaut, A., Smolders, I., and De Bundel, D. (2019). The Barnes maze task reveals specific impairment of spatial learning strategy in the intrahippocampal kainic acid model for temporal lobe epilepsy. Neurochem. Res. *44*, 600–608. https://doi.org/10.1007/s11064-018-2610-z.

114. Twele, F., Töllner, K., Bankstahl, M., and Löscher, W. (2016). The effects of carbamazepine in the intrahippocampal kainate model of temporal lobe epilepsy depend on seizure definition and mouse strain. Epilepsia Open *1*, 45–60. https://doi.org/10.1002/epi4.2.

115. Twele, F., Schidlitzki, A., Töllner, K., and Löscher, W. (2017). The intrahippocampal kainate mouse model of mesial temporal lobe epilepsy: lack of electrographic seizure-like events in sham controls. Epilepsia Open *2*, 180–187. https://doi.org/10.1002/epi4.12044.

116. Faul, F., Erdfelder, E., Lang, A.G., and Buchner, A. (2007). G*Power 3: a flexible statistical power analysis program for the social, behavioral, and biomedical sciences. Behav. Res. Methods *39*, 175–191. https://doi.org/10.3758/bf03193146.

STAR★METHODS

KEY RESOURCES TABLE

REAGENT or RESOURCE	SOURCE	IDENTIFIER
Antibodies and FISH probes		
Alexa488_Donkey anti chicken	Jackson Immunoresearch Laboratories, Inc	Cat# 703-546-155; RRID:AB_2340376
Alexa488_Donkey anti goat	Thermo Fisher Scientific	Cat# A-11055; RRID:AB_2534102
Alexa488_Donkey anti guinea pig	Jackson Immunoresearch Laboratories, Inc	Cat# 706-546-148; RRID:AB_2340473
Alexa488_Donkey anti sheep	Jackson Immunoresearch Laboratories, Inc	Cat# 713-546-147; RRID:AB_2340746
Alexa546_Donkey anti rabbit	Thermo Fisher Scientific	Cat# A10040; RRID:AB_2534016
Alexa647_Donkey anti mouse	Thermo Fisher Scientific	Cat# A-31571; RRID:AB_162542
BRACHYURY (D2Z3J)	Cell Signaling Technology	Cat# 81694; RRID:AB_2799983
CALB	Swant	Cat# 300; RRID:AB_10000347
CASP3 (Asp175)	Cell Signaling Tehchnology	Cat# 9661; RRID:AB_2341188
CHAT (FISH probe)	Thermo Fisher	Assay ID: VA1-11432-PF
Control-dapB AF488	Thermo Fisher	Assay ID: VF4-10408-PF
Control-dapB AF647	Thermo Fisher	Assay ID: VF1-11712-PF
COUPTFII	Cosmo Bio	Cat#PPH714700; RRID:AB_567523
CR	Swant	Cat# 6B3; RRID:AB_10000320
CXCR4	R&D Systems	Cat# FAB173A; RRID:AB_357081
DAPI Fluoromount-G	Southern Biotech	Cat#0100-20
DCX	Millipore	Cat# AB2253; RRID:AB_1586992
Click-iT Plus EdU Alexa Fluor 647 Imaging Kit	Thermo Fisher Scientific	Cat#C10640
ERBB4	R&D Systems	Cat# AF1131; RRID:AB_354620
FOXG1	Takara	Cat# M227; RRID:AB_2827749
GATA4 (D3A3M)	Cell Signaling Technology	Cat# 36966; RRID:AB_2799108
GFP	Aves Labs	Cat# GFP-1020; RRID:AB_10000240
GLAST	Miltenyi Biotec	Cat# 130-095-822; RRID:AB_10829302
hGAD1 (FISH probe)	Advanced Cell Diagnostics	404031-C3
hGAPDH (FISH probe)	Advanced Cell Diagnostics	442201-C2
hMAP2	Abcam	Cat# ab5392; RRID:AB_2138153
HNA	Millipore	Cat# MAB1281; RRID:AB_94090
Hoechst 33342	Fisher Scientific	H3570
hTAU	BioLegend	Cat# 835201; RRID:AB_2565341
ISL1	Neuromics	Cat# GT 15051; RRID:AB_2314682
Ki67	Dako	Cat# M7240; RRID:AB_2142367
KU80	Abcam	Cat# ab80592; RRID:AB_1603758
LHX6	Santa Cruz Biotechnology	Cat# sc-271433; RRID:AB_10649856
LHX8	Thermo Fisher Scientific	Cat# PA5-67201; RRID:AB_2663645
LHX8 (FISH probe)	Thermo Fisher	Assay ID: VA1-3018704
MAF	Santa Cruz Biotechnology	Cat# sc-7866; RRID:AB_638562
MAF (FISH probe)	Thermo Fisher	Assay ID: VA1-17805-PF
MAFB	Sigma-Aldrich	Cat# HPA005653; RRID:AB_1079293
MAP2	Abcam	Cat# ab5392; RRID:AB_2138153
MEF2C	Cell Signaling Technology	Cat# 5030; RRID:AB_10548759
MIB-1	Dako	Cat# M7240; RRID:AB_2142367
NANOG	R&D Systems	Cat# AF1997; RRID:AB_355097
NEUN	Millipore	Cat# ABN91; RRID:AB_11205760
NKX2-1	Leica Biosystems	Cat# NCL-L-TTF-1; RRID:AB_564042

(*Continued on next page*)

Continued

REAGENT or RESOURCE	SOURCE	IDENTIFIER
NKX2.2	DSHB	Cat# 74.5A5; RRID:AB_531794
NPY	Millipore	Cat# AB1583; RRID:AB_2236176
OCT4	Santa Cruz Biotechnology	Cat# sc-5279; RRID:AB_628051
OCT4 [AF488]	BD Biosciences	Cat# 560253; RRID:AB_1645304
OLIG2	Millipore	Cat# AB9610; RRID:AB_570666
OTX2	Neuromics	Cat# GT15095-100; RRID:AB_2157174
PAX6	Biolegend	Cat# 901301; RRID:AB_2565003
PROX1	R&D systems	Cat# AF2727; RRID:AB_2170716
PV	Swant	Cat# GP72; RRID:AB_2665495
SOX1	R&D systems	Cat# AF3369; RRID:AB_2239879
SOX10	R&D Systems	Cat# AF2864; RRID:AB_442208)
SP8	Abcam	Cat# ab73494, RRID:AB_2050331
SST	Peninsula Laboratories	Cat# T-4103.0050; RRID:AB_518614
SST (FISH probe)	Thermo Fisher	Assay ID: VA4-10836-PF
STEM121 (HMNA)	Takara	Cat# Y40410; RRID:AB_2801314
STEM123 (hGFAP)	Takara	Cat# Y40420; RRID:AB_2833249
TRA1-60 [PE-Cy7]	Biolegend	Cat# 330620; RRID:AB_2728286
VGAT	Synaptic Systems	Cat# 131 003; RRID:AB_887869
VGAT (FISH probe)	Thermo Fisher	Assay ID: VA4-3098129-PF
VIM	Invitrogen	Cat# PA1-10003; RRID:AB_2216267
WFA	Vector Laboratories	Cat# B-1355; RRID:AB_2336874
Anti-Biotin MicroBeads	Miltenyi Biotec	Cat# 130-105-637; RRID:AB_2811216
ERBB4-Biotinylated	R&D Systems	Cat# BAF1131; RRID:AB_355862
Biological samples		
iCell GABAergic Neurons	FUJIFILM Cellular Dynamics	C1008
GABAergic Neurons	BrainXell	BX-0400
spinal motor neurons	BrainXcell	BX-0100
FUGW (Lenti-hUbC-EGFP)	Lois et al.[100]	RRID:Addgene_14883
pLenti-Synapsin-ChR2(H134R)-EYFP-WPRE	Zhang et al.[101]	RRID:Addgene_20945
Chemicals, peptides, and recombinant proteins		
ReLeSR	STEMCELL Technologies	100-0484
StemPro Accutase	Life Technologies	A1110501
TrypLE™ Select Enzyme	Fisher Scientific	12563029
Fibronectin	Sigma Aldrich	F2006
Laminin	R&D Systems	3400 -010 -02
Matrigel (GFR)	Fisher Scientific	CB-40230
Poly-L-Ornithine	Sigma Aldrich	P3655
Vitronectin	Life Technologies	A27940
B-27 without Vitamin A	Life Technologies	12587-010
D-PBS	Fisher Scientific	14190144
Distilled Water	Fisher Scientific	15230147
DMEM/F12	Life Technologies	21331
Essential 8 medium kit	Life Technologies	A2656101
GlutaMAX	Life Technologies	35050-061
L-Ascorbic Acid	Sigma Aldrich	A5960
MEM non-essential amino acids	Life Technologies	11140-050
N2 supplement-B	Stem Cell Technologies	7156
Neurobasal-A	Life Technologies	10888

(*Continued on next page*)

Continued

REAGENT or RESOURCE	SOURCE	IDENTIFIER
Penicillin-Streptomycin	Life Technologies	15140-122
β-Mercaptoethanol	Life Technologies	21985-023
Benzonase	Sigma Aldrich	1016970001
DAPT	Tocris	2634
Kainic acid	Tocris	0222
LDN193189	Tocris	6053
PD0325901	Tocris	4192
PD0332991	Selleck Chem	S1116
SAG	Tocris	4366
SB431542	Tocris	1614
XAV939	Tocris	3748
Y27632	Tocris	1254
Deposited data		
Raw data of Fastq files for scRNA-seq experiments	This Paper	GEO: GSE208672
Codes for process the scRNA-seq data	This Paper	https://doi.org/10.7910/DVN/T66DMY
Public scRNA-seq of human ganglionic eminences	Shi et al.[70]	GEO: GSE135827
Experimental models: Organisms/strains		
NOD.Cg-PrkdcscidIl2rgtm1Sug/JicTac	Taconic	NOG- OF-M- HOM;HEMI
Software and algorithms		
Cell Ranger v3.1.0	10x Genomic	support.10xgenomics.com
Seurat v3.2.2	Stuart et al.[102]	satijalab.org/seurat/
R version 4.0.3	The R Project for Statistical Computing	www.r-project.org/

RESOURCE AVAILABILITY

Lead contact

Further information and requests for resources and reagents should be directed to and will be fulfilled by the lead contact, Cory Nicholas (cory@neuronatx.com).

Materials availability

Reagents utilized in this study that are not commercially sold will be made available upon reasonable request (consideration will be given to limited quantity and availability of suitable alternatives).

Data and code availability

Single-cell RNA-seq data (original and reanalyzed) have been deposited in NCBI's Gene Expression Omnibus (GEO) and are publicly available as of the date of publication. Accession numbers are listed in the key resources table. All original code has been deposited at Harvard Dataverse and is publicly available as of the date of publication. DOIs are listed in the key resources table. Any additional information required to reanalyze the data reported in this paper is available from the lead contact upon request.

EXPERIMENTAL MODEL AND STUDY PARTICIPANT DETAILS

Institutional oversight

All activities, procedures and materials used were reviewed and approved by Neurona's Stem Cell Research Oversight Committee and Institutional Animal Care and Use Committee.

hESC line and banks

The MGE-type pallial GABAergic inhibitory interneurons described in this study were differentiated from research-grade working cell banks derived from a cGMP-grade human embryonic stem cell (hESC) line. The cell line is listed in the NIH hESC Registry as an ''Approved Line'' (eligible for use in NIH-supported research). Donor consent was obtained for use of the cells in research, clinical and commercial development. Donor screening was performed using FDA's Donor Eligibility Guidelines for HCT/Ps. The cell line was derived, expanded, and banked under cGMP conditions using qualified raw materials to generate a GMP seed cell bank (SCB), research-grade master cell banks (rMCB) and working cell banks (rWCB). Karyotypic analysis and pluripotency marker expression were assessed across all hESC cell banks, demonstrating genomic stability and high purity. The pluripotent stem cell

banks were tested for sterility and found negative for relevant viruses, mycoplasma, and adventitious agents. Pluripotency of the undifferentiated cells was demonstrated by expression of markers such as TRA-1-60, OCT-4, and NANOG; the in vitro differentiation of the cells to endoderm, ectoderm, and mesoderm lineage; and the demonstration of teratoma formation when undifferentiated hESCs were engrafted *in vivo*.

hESC stability

The hESC WCBs were tested for genetic stability per ICH Q5D(ICH_Q5D 1998) by evaluating the cell substrate for consistent production of the intended cell fate. MGE-type patterning and differentiation to pallial interneurons using the manufacturing process was initiated from rWCB ESCs after up to five additional passages of ESC expansion to reflect the intended limit of cultivation, and genetic stability was characterized using the complementary orthogonal methods of karyotype analysis by G-banding and single nucleotide polymorphism (SNP) arrays. Since the product being manufactured is post-mitotic and karyotype analysis by G-banding requires mitotic cells, karyotype analysis was performed during the ESC expansion, and genome-wide genomic copy number variants (CNVs) and regions of homozygosity analysis (ROH) were assessed during both ESC expansion and end-of-process (EOP) interneuron differentiation using SNP arrays.

In addition, we performed exon capture, next generation sequencing and variant analysis of the TP53 gene using gDNA isolated from ESCs and EOP interneurons, with at least 100X on target coverage. Libraries were prepared using CleanPlex® TP53 Panel (Paragon Genomics) and sequenced on the Illumina platform and analyzed by ACGT Inc for TP53 mutations recurrently acquired in human pluripotent stem cells during in vitro culture.[103] The characterizations demonstrated:

a. no genetic abnormality occurs during ESC expansion or following the interneuron production process from ESCs at the maximum limit of in vitro cultivation; and
b. consistent production of the intended pallial interneuron cell product at the maximum limit of in vitro cultivation.

Animals

All efficacy studies were non-GLP studies. Activities described in this report were performed in accordance with the active Neurona Therapeutics IACUC protocol covering temporal lobe epilepsy and adhered to the ARRIVE guidelines.[104]

Up to 85 NOG (NOD.Cg-*Prkdc*^{scid}*Il2rg*^{tm1Sug}/JicTac) male mice per study were obtained from Taconic in the range of approximately 5-6 weeks of age for comparisons of different cell lots or doses and vehicle groups. Male mice were chosen because they display more consistent seizures in this model.[105] Mice were assigned a unique identifier number on arrival, which was marked on the mouse by ear-notches and tail tattoos. Animals were maintained in the Neurona Therapeutics Animal Facility under standard temperature and humidity on a 12:12 light/dark cycle. Bottled water and standard chow were provided ad libitum. Single-use cages were used with irradiated Alpha-Dri bedding. Prior to induction, animals were co-housed when possible. Colony health was monitored through monthly diagnostic sample submission for microbiology. All described surgical procedures were accompanied by meloxicam (Metacam® 10 mg/kg in 2mL/kg i.p.) as a non-steroidal anti-inflammatory drug, antibiotic enrofloxacin (Baytril® 10 mg/kg in 4.4 mL/kg s.c.), and local anesthesia on the scalp with bupivacaine (2.5 mg/kg in 5 mL/kg s.c.). After every surgery, animals received 1 mL warmed Ringer's solution s.c. to rehydrate, and their cages were placed on a heating pad until full recovery from anesthesia.

METHOD DETAILS

hESC expansion

A cGMP grade hESC line was adapted to a feeder-free, xeno-free culture system using human recombinant vitronectin (A27940, Life Technologies) coated dishes, Essential 8 medium kit (A2656101, Life Technologies) and dissociation reagent ReLeSR (100-0484, STEMCELL Technologies). Media was changed daily, and cells were passaged every 5 days, for a total of 5 passages, before being cryopreserved to sequentially generate a GMP SCB, and research-grade rMCBs and rWCBs.

MGE pallial-type interneuron differentiation

For each differentiation experiment, one vial of rWCB was thawed. The thawed hESCs were seeded into adherent culture and expanded for 5 days post-thaw using conditions described above. To initiate differentiation, the expanded hESCs were dissociated into a single cell suspension using StemPro Accutase (A1110501, Life Technologies) and resuspended in differentiation media consisting of Neurobasal-A (50%; 10888, Life Technologies) and DMEM/F12 (50%; 21331, Life Technologies), supplemented with GlutaMAX (1X; 35050-061, Life Technologies), B-27 without Vitamin A (1X; 12587-010 Life Technologies), N2 supplement-B (1X; 07156, Stem Cell Technologies), Penicillin-Streptomycin (1X; 15140-122, Life Technologies), L-Ascorbic Acid (200μM; A5960, Sigma), β-Mercaptoethanol (55M; 21985-023 Life Technologies), and MEM non-essential amino acids (1/2X; 11140-050, Life Technologies). The resuspended hESCs were exposed to patterning and differentiation cues from day 0, adjusting small molecule combinations over time and changing media every 2 to 3 days, using only chemically-defined reagents and small molecules, in the absence of knockout serum replacement (KSR).

During the three main protocol phases (Figure S2A), small molecules modulating the listed cell signaling pathways were introduced to promote robust MGE patterning and differentiation into pallial-type GABAergic interneurons. During the neuroectoderm

specification and MGE patterning phase, ROCK inhibitor (Y27623 10μM; 1254 Tocris) with TGFβ and BMP pathway inhibition induced neuroectoderm (SB431542 10μM; 1614 Tocris / LDN193189 250nM; 6053 Tocris).[38,40,106] WNT pathway inhibition conferred forebrain identity (XAV939 10μM; 3748 Tocris)[107,108] and SHH pathway activation induced ventral forebrain MGE-like progenitors (SAG 100nM; 4366 Tocris).[37,38,40,43,107] During the second MGE progenitor expansion and pallial interneuron commitment phase, a MEK pathway inhibitor was applied to further improve the efficiency, kinetics, and specificity of a pallial-type GABAergic interneuron lineage (PD0325901 2μM; 4192 Tocris). Finally, during the third phase, inhibitors of the MEK (PD0325901 2μM; 4192 Tocris), CDK (PD0332991 2μM; S1116 Selleck Chemicals)[44,109] and NOTCH (DAPT 10μM; 2634 Tocris)[40,43,45] pathways were added to induce cell cycle exit and differentiation into post-mitotic MGE-type pallial GABAergic interneurons. The experiments described herein used research-grade WCBs and derived pallial interneuron cell lots, and do not represent the clinical candidate (NRTX-1001) that is being evaluated in a clinical trial for drug-resistant epilepsy.

Cell batch processing and cryopreservation

At the end of the differentiation process, cells were harvested and dissociated to single cells using TrypLE™ Select Enzyme and Benzonase (1/10000; Sigma Aldrich). A portion of the harvested cell suspension was subsequently processed for ERBB4 positive selection using magnetic-activated cell sorting (MACS). Single cell suspension was incubated with a biotinylated primary antibody against human ERBB4 (BAF1131 R&D Systems), followed by incubation with Anti-Biotin MicroBeads (130-105- 637, Miltenyi Biotec), and magnetic sorting was performed on the CliniMACS according to manufacturer instructions (Miltenyi Biotec). Unsorted (pre-sort) and sorted (post-positive selection) cell populations were cryopreserved using the CryoMed controlled-rate freezer (Fisher Scientific), before further storage in vapor-phase liquid nitrogen.

Immunocytochemistry

Thawed cells were counted using the NC-200 cell counter (Chemometec) and seeded into 384-well plates coated with Poly-L-Ornithine/Fibronectin/Laminin (PO/Fib/Lam) at ~4.0E5-4.3E5 cells/cm^2. Cells were fixed with 4% paraformaldehyde (PFA) for 10 minutes between 3-16 hours after plating and processed for staining within two weeks. Briefly, cells were incubated with a blocking buffer (10% donkey or goat serum, 0.1% Triton X-100 in DPBS (Dulbecco's phosphate-buffered saline)) for 30 minutes at ambient temperature. Primary and secondary antibody dilutions were prepared in blocking buffer and kept on ice. Primary antibody incubation occurred at 4°C overnight, followed by two 30-minute washes with PBS-T (DPBS, 0.1% Triton X-100). Secondary antibody (Alexa Fluor conjugated, Life Technologies) incubation occurred at ambient temperature in the dark for 2 hours, followed by two 30-minute washes with PBS-T. The second wash was replaced with DPBS for imaging and storage. Aspiration and washes in 384-well plates were automated using the plate washer ELX406 (Biotek). Images were acquired using the Leica DMi8 microscope with a 20X objective. A minimum of 3-5 fields of view were captured (typically 250-350 cells per field) for each sample and antibody combination. Analysis was performed manually using ImageJ software. For higher throughput sample images acquisition, analysis and quantification, the automated high content screening imaging system CX5 (Life Technologies) was used. Independent combinations of antibodies (up to 4 independent channels for the detection of Hoechst, Alexa Fluor (AF)488, AF547 and AF650)) were acquired independently with specific exposure times. Adjusting background correction and segmentation parameters, and using "spot detector" bio application, nuclei were identified as primary objects to define regions of interest on subsequent channels, and to determine percent of positive cells expressing a given marker, based on morphological and intensity thresholding.

Assessment of residual pluripotent cells by flow cytometry

Cells were stained on day 28 and at the end of process (post-thaw) with PE/Cy7 anti-human-TRA-1-60 (Biolegend) for surface TRA-1-60, Fixable Far Red dye (ThermoFisher Scientific) for viability and AF488 anti-human-OCT4 (BD Bioscience) for intracellular OCT4. The cells were analyzed using an Attune-NxT Acoustic Focusing Flow Cytometer and data were analyzed using FlowJo (BD Biosciences) software. To assess the presence of residual pluripotency markers in the final cryopreserved product, an extensive qualification was performed to determine the assay repeatability, accuracy, linearity and limits of detection (LOD) per ICH Q2 guidelines. Samples were stained in triplicate (1E7 cells per sample) for better population statistics. From this study we determined the method is accurate in detecting pluripotent cells at a LOD of 0.002%. When the method was employed to analyze samples at the end of the process, the percentage of pluripotent cells detected was always below the LOD.

Primeflow

Cells were thawed, counted using the NC-200 cell counter, stained using Fixable Aqua Dead Cell Stain Kit (Life Technologies, cat# L34957), and processed for RNA Primeflow assay (Thermo Fisher, cat# 8818005-210) according to the manufacturer's instructions. Reactions were run in triplicate. Data were acquired using the Attune NxT Flow Cytometer (Life Technologies). All events in the sample were recorded (in the range of 6E4-3E5) and results were analyzed using the FlowJo software. Fixable Aqua and FSC were used to gate live cells. Single cells were then gated on forward scatter area and height (FSC-A versus FSC-H) and side scatter area and height (SSC-A versus SSC-H). Using dapB as the negative control, gates were set in histogram plots for AF488 and AF647 probes. The same gates were then applied to all the test samples accordingly to determine the percentage of expression in cell lots. Quantitative results were reported as the average ± standard deviation of 3 technical replicates.

GABA release

To perform the GABA release assay, cryopreserved cells were thawed and seeded onto a PO/Fibronectin/Laminin-coated 96-well plate at a density of 6.5E5 cells/cm2 in culture media. Each cell lot was seeded in six wells, and cells were cultured at 37°C, 5% CO2 for 8 days, with media changes every 2-3 days. On day 8, spent medium was replaced with fresh pre-warmed medium either alone or supplemented with 90 mM potassium chloride (in triplicate wells per condition). After a 30-minute incubation at 37°C, 5% CO2, cell-free supernatants were collected and stored at -80°C. The samples were submitted for liquid chromatography and mass spectrometry (LC/MS-MS) analysis of GABA and acetylcholine (ACh) neurotransmitter content (Charles Rivers Laboratories). To confirm functional specificity, the GABA release assay was performed using hESCs and commercial spinal motor neurons (SMNs, BrainXcell), neither of which normally secrete GABA. hESCs were seeded at a density of 2.5E4 cells/cm^2 in E8 media containing ROCK inhibitor for 72 hours prior to sample collection. One day post-seeding, the media was changed to the same neuronal culture media as hESC-derived interneurons, and the cells were fed daily until sample collection. SMNs were thawed and seeded into a polyornithine/fibronectin/laminin coated 96-well plate at a density of 6.5E5 cells/cm^2 and cultured for 8 days as described by the manufacturer. The sample collection was performed the same way for ESCs and SMNs as for the hESC-derived interneurons on day 8.

In vitro cell migration

To assess the migration potential of hESC-derived pallial MGE-type interneurons compared to human fetal MGE-derived interneurons and other in vitro-derived GABAergic cell preparations, a migration assay was developed, in which cells were aggregated and embedded into a MatrigelTM (CB-40230, Fisher Scientific) drop covered with culture medium, and then incubated for three days to allow for the visualization and quantification of cells migrating away from the main cell aggregate. Primary human MGE was dissected from mid-gestational age tissue (GW18-20) followed by dissociation and sorting for ERBB4. All hPSC-derived interneurons were thawed prior to aggregation. The commercial sources of hPSC-derived GABAergic cells were from Cellular Dynamics International (vendor "X": iCell GABA Neurons, cat #C1008) and BrainXell (vendor "Y": GABAergic Neurons, cat #BX-0400). Cells from different sources were prepared by one operator, assigned a random ID and handed to a different operator de-identified for assays and data analyses.

To perform the migration assay, 5E3 cells in 100 μl of culture medium were spun down in 96-well V bottom plates (S-bio, MS-9096VZ) and allowed to aggregate at 37°C, 5% CO_2 over a period of three days. The aggregates were then embedded into a 5 μL MatrigelTM drop in the center of a 96-well flat bottom assay plate with the aid of a dissecting microscope inside the biosafety cabinet (BSC) (one aggregate per well, twelve aggregates per sample). After a 15-minute incubation at ambient temperature, 200 μl of culture medium was added to the wells, followed by incubation at 37°C, 5% CO_2 for three days. On day 3 of migration, samples were fixed for 30 minutes with a 2% PFA and 1X Hoechst solution at ambient temperature, protected from light. The fixation solution was washed away three times using DBPS, keeping samples immersed in DPBS at all times. Migration images were acquired using the CX5 instrument with a 4X objective, projecting the maximum intensity across 375 μm (15 z-plans, 25 μm steps). The number of Hoechst positive cells that migrated away from the aggregate was quantified automatically using "spot detector" bio application. Percentage of migrating cells was determined based on the number of Hoechst positive spots detected divided by 5E3 (input cells that were aggregated).

Single cell RNA sequencing

To objectively assess cell composition, scRNA-seq analysis was performed using the 10X Genomics platform on the hESCs prior to the start of differentiation, hESC-derived MGE-type VZ-like progenitors on day 14 of differentiation, and nine independent unsorted cell lots at the end of the differentiation process. For three of the lots, including lots 1 and 2 used in efficacy studies, the corresponding sorted lots were also sequenced. All samples were thawed the day of capture and transported on ice to SeqMatic (Fremont, CA) for downstream processing and data generation. Individual cells were captured and barcoded using the chromium controller, cDNA libraries were prepared using next GEM 3' V3.1 kits (10x Genomics), cDNA libraries were quantified using the Agilent Tapestation 4200 and pooled for sequencing. Pooled libraries were quantified using Lightcycler 96 qPCR and sequenced by the Illumina NovaSeq 6000. Typically, ~8E3-1.2E4 cells were captured per sample. About 200 million reads were obtained for each sample, with an average read depth of ~20,000 reads per cell. Cell Ranger v3.1.0 (10x Genomics) was used to demultiplex FASTQ files for each sample, align reads to the human GRCh38 genome downloaded from 10x Genomics, and quantify the expression levels for each gene in each cell from each sample. R version 4.0.3 and Seurat v3.2.2 were used to quality control, normalize, cluster, and visualize the cells from all samples. Cells were filtered for quality by having at least 1000 expressed genes, at least 1000 unique reads, no more than 20% reads of mitochondrial genes and no more than 40% reads of ribosomal genes. Cells were normalized by the 'LogNormalize' method. The top 3000 genes were identified by 'FindVariableFeatures' with 'vst' selection method for downstream integration analysis. Seurat CCA (Canonical Correlation Analysis) integration workflow was applied to remove the batch effects between different cell lots. hESCs and Day 14 progenitors were merged with the integrated differentiated lots for clustering. PCA (Principal component analysis) was applied, 30 PCs (principal components) were selected, and cells were clustered with Seurat standard workflow. Using a dimension reduction technique called UMAP (Uniform Manifold Approximation and Projection), cells were visualized in a 2-dimensional space and colored by groups, where each dot represents one cell, and groups of cells with similar gene expression

form into clusters. Top markers for each cluster were identified by using the Seurat 'FindAllMarkers' function with ROC method and the cell type of each cluster were determined by the expression of typical cell markers of each type. Gene expression was visualized with violin-plot, dot-plot and feature-plot built in Seurat package.

To compare and classify in vitro hESC-derived interneurons with published data, human developing GE snRNAseq data were downloaded from GEO dbs,[70] and processed to identify MGE, CGE, LGE and other clusters as described in the original report. PCA and UMAP models of cell types were computed and the human developing GE reference was constructed by following the Seurat reference mapping procedure. The cell type classification of hESC-derived interneurons was assigned based on prediction scores using the human GE cells as a reference. Each in vitro cell was assigned a score between 0 and 1 for each cell type based on the transcriptomic similarity between the query and the reference (human developing GE cells). The prediction scores of each cell for each cell type category were projected onto UMAP clusters and the predicted-cell-type compositions (percentage) for each cluster were visualized with the heatmap.

Epilepsy induction

After acclimation of 2 weeks, animals received 0.21 μg kainic acid (KA; Tocris) dissolved in 50 nL NaCl into the right dorsal HC to induce epilepsy[110] ((coordinates in relation to Bregma: AP -2.0; ML +1.6; DV -1.65), using a pulled glass needle with 70-90 μm diameter at the tip and a connected microinjection system (Narishige). At this first surgery, the body weight of the animals was 23-24 g on average. After injection of KA, mice were kept under isoflurane anesthesia for a total of 1 hour to avoid the more severe seizures associated with recovery from inhaled anesthesia.[105] After recovery from anesthesia, animals were closely monitored for occurrence of generalized seizures. All mice began seizing within 90 min post-anesthesia and were then returned to the animal housing room in single-housed cages. Status epilepticus (SE) was not interrupted in this model.[79] Mice were injected with 1 mL lactated Ringer's solution to ensure rehydration during/after SE. Additionally, food pellets and water as a gel were provided at the bottom of the cage. If necessary, mice were placed on heating pads and manually provided with Ensure® liquid diet supplement on the day after SE. If failure to thrive was observed, the mouse was euthanized. Mortality during and within the first days after SE was <10%.

Cell transplantation into the MTLE mouse model

Transplantation of hESC-derived MGE-type pallial interneurons or vehicle (serum-free base medium) was performed four to five weeks after SE induction to ensure that the mice displayed spontaneous seizures and were chronically epileptic prior to treatment.[79,105] Cells were transplanted using the same system as for the KA injections, a pulled glass needle with 70-90 μm diameter at the tip and a connected microinjection system (Narishige). Cells were injected in 4-6 different deposits (AP -1.85, ML 1.7, DV -1.7; AP -2.5, ML 2.65, DV -1.9; AP -3.15, ML 2.6, DV -2.2; AP -3.15, ML 3.05, DV -3.7; DV coordinates are in relation to brain surface) per brain hemisphere in a dose of 5E3 (5K) - 6E5 (600K) cells per deposit depending on the target dose from 2.5E4 (25K) to 1.5E6 (1.5M) per hemisphere. After delivery of the hESC-derived interneurons, the needle remained in the tissue for approximately 30 seconds to prevent backflow of cell suspension along the needle tract. Control mice received similar amounts of vehicle solution into the same deposit coordinates.

Electrode implantation and EEG recording

For recording an electroencephalogram (EEG), transmitters from Data Science International (DSI) were implanted and connected in-house to a custom-made bipolar electrode (PlasticsOne). The DSI transmitter was implanted subcutaneously over the left flank of the mouse and the electrode was lowered into the right dorsal CA1 of the HC into the same site as the previous KA injection (coordinates in relation to Bregma: AP -2.0; ML +1.6; DV -1.65). The electrode was secured in the skull by implanting three holding screws (2 rostral, 1 caudal) and Loctite glue. Implantation happened in the same surgery as cell/vehicle transplantation or within a few weeks of transplantation surgery. Electrode implantation prior to cell transplantation was not possible because this would have required the intrahippocampal electrode to be removed and reimplanted. After DSI transmitter implantation, EEG and video recordings (Ponemah; DSI) were acquired in multi-day 24-hour sessions for each animal enrolled in the study; the data were saved to a server approximately daily and archived at least monthly on backup storage hard drives. EEG was recorded 24/7 for 1-3 weeks at various time points post-SE using Ponemah software. Recording time points for most studies were between 1-2 MPT, 5 MPT, and 7 MPT. Some studies (lot 3S & 4S) were recorded also at earlier and later time points (Figure S5).

Criteria for exclusion

Animals that did not display behavioral seizures (SE) within 2 hours after intrahippocampal kainate injection were removed from the study. Animals were also excluded if EEG quality was too poor to detect electrographic seizures or if animals did not display epileptiform activity at any recording time point after cell transplantation. If an animal's EEG trace was confounded by heartbeat or EMG with no clear EEG (seizures/spikes deriving from brain activity), it was excluded from the study. If an animal's EEG trace displayed continuous spiking (sign of generalized seizure activity), it was excluded on that day. If an EEG could not be analyzed for at least 4 days at one recording time point, the animal would be excluded from the respective time point. In the case of EEG traces that displayed increased interictal activity and/or generalized seizures and in rare cases in which animals had a high generalized seizure frequency (>3 seizures/day), they were excluded from analysis of electrographic seizures. Exclusion of data was performed prior to unmasking to treatment. If an animal did not survive to the endpoint of the study, the EEG data were collected and analyzed up to the point of animal's death and all data were maintained in the study files.

Brain slice electrophysiology

For electrophysiology studies, cells were seeded onto PO/Fib/Lam coated multiwell plates in culture media. Following overnight incubation at 37°C, 5% CO2, culture medium was replaced with fresh medium containing lentivirus supernatants (FUGW = Lenti hUbC-EGFP or pLenti-Syn-hChR2-EYFP) based on the optimal titration that was determined empirically in a separate experiment to achieve 95% EGFP+ or YFP+ expression. After a three-day incubation, culture medium was removed followed by three washes with PBS to remove any residual viral particles. Cells were harvested using 0.25% trypsin solution, quenched with FBS (20% final). Upon harvesting, cells were concentrated by centrifugation (150g, 4 minutes at room temperature). Concentrated cell suspension (approx 1E6/μl) was loaded into beveled glass micropipettes (internal diameter ≈80-90 μm, Wiretrol 5 μl, Drummond Scientific Company) prefilled with mineral oil and mounted on a microinjector. Concentration of the cell suspension within the needle was determined using a hemocytometer just prior to the injection. Postnatal day (P)0-2 Scid-beige (CRL) mice were anesthetized by hypothermia for 1-2 minutes and subsequently positioned in a clay mold to stabilize the head. Recipient mice were injected 3 times bilaterally with 50E3 cells/injection site (total = 300E3 cells per pup). Injections were performed 0.75, 1.25, 2.5 mm anterior from Lambda, 0.75, 1.0, 1.0 mm away from the midline (respectively) and at a depth of 0.35 mm from the surface of the skin. After the injections were completed, the needle was slowly removed and transplant recipients were placed on a warm surface to recover from hypothermia. The mice were then returned to their mothers until they were weaned (P21).

Adult (6-8 weeks old) NOG male mice were transplanted as described above. A total dose of 200E3 cells/HC was delivered into the mouse HC at 4 different sites (50E3 cells/injection) with respect to bregma (AP: -1.85; ML: +1.8; DV: -1.7 mm; AP: -2.5; ML: +2.65; DV: -1.9 mm; AP: -3.15; ML: +2.8; DV: -2.4 mm and AP: -3.15; ML: +3.25; DV: -3.45 mm). Mice up to one year of age were deeply anesthetized with intraperitoneal injection of freshly prepared Avertin (250 mg/kg) and perfused with ice-cold sucrose-based solution (210 mM Sucrose, 2.5 mM KCl, 10 mM MgSO4, 2 mM CaCl2, 1.25 mM NaH2PO4, 24 mM NaHCO3, 11 mM glucose). The brain was removed and sectioned into 300 μm thick slices, which were transferred to 34°C ACSF (126 mM NaCl, 3 mM KCl, 2 mM MgCl2, 2 mM CaCl2, 1.2 mM NaH2PO4, 26 mM NaHCO3, 10 mM glucose) for 30 minutes at room temperature for no more than 6 hours for later use.

For older animals, we adapted a previously published "protective recovery method.[111]" Mice were deeply anesthetized and transcardially perfused with ice-cold "NMDG-HEPES aCSF" (92 mM NMDG, 92 mM HCl, 2.5 mM KCl, 1.2 mM NaH2PO4, 30 mM NaHCO3, 20 mM HEPES, 25 mM glucose, 5 mM sodium ascorbate, 2 mM thiourea, 3 mM sodium pyruvate, 10 mM MgSO4, 0.5 mM CaCl2). The brain was dissected and sectioned into 300 μm coronal slices. Slices were transferred to 34°C "NMDG-HEPES aCSF" for 40 minutes to recover. During the recovery phase, Na+ spike-in solution (2 M NaCl in NMDG-HEPES aCSF) was added at the following time points: 15 min: 0.25 mL; 20 min: 0.25 mL; 25 min: 0.5 mL; 30 min: 1 mL; 35 min: 2 mL. Slices were then stored in "HEPES holding aCSF" (92 mM NaCl, 2.5 mM KCl, 1.2 mM NaH2PO4, 30 mM NaHCO3, 20 mM HEPES, 25 mM glucose, 5 mM sodium ascorbate, 2 mM thiourea, 3 mM sodium pyruvate, 2 mM MgSO4, 2 mM CaCl2) at room temperature for no more than 6 hours for later measurements in "recording aCSF" (124 mM NaCl, 2.5 mM KCl, 1.2 mM NaH2PO4, 24 mM NaHCO3, 5 mM HEPES, 12.5 mM glucose, 2 mM MgSO4, 2 mM CaCl2). All solutions were balanced for 30 minutes with carbogen (95% O2, 5% CO_2) before use.

Borosilicate glass pipettes (4-8 MOhm) were backfilled with a solution containing: 140 mM K-gluconate, 2 mM MgCl2, 10 mM HEPES, 0.2 mM EGTA, 4 mM MgATP, 0.3 mM NaGTP, 10 mM Phosphocreatine d-tris, and 0.25% (g/100mL) biocytin. Signals were collected at room temperature at a sampling rate of 50K, filtered using a 10K bessel filter (MultiClamp 700B, Axon Instruments, Molecular Devices) and digitized (Digidata 1320A, Axon Instruments, Molecular Devices). Recording data were further filtered using Clampfit (v10.7), "Lowpass" function with Gaussian type and 2000 Hz -3 dB cutoff. Stimfit (0.15.8, https://github.com/neurodroid/stimfit) and python were used to calculate and plot the parameters.

Behavior

For all assays, experimenters were masked to animal treatment group, and test order was based on the experimenter randomly selecting a cage. Modified Irwin's Test: General health and wellness of the animals was assessed using a modified Irwin screen adapted from a protocol used to test safety and tolerability of anti-seizure drugs in naive and epileptic mice.[112] An animal's sensitivity to touch, noise, tail elevation, and spatial locomotion (mobility) were evaluated, as well as their body position and fur condition. A value of 2 was set as the usual expected reaction for a healthy mouse in the test. Animals were tested in an empty mouse cage in their housing room. One experimenter administered the test while two other experimenters scored the animal or its reaction. Animals were assessed at least twice during the study. If an animal had a generalized seizure during the test, it was excluded. The two evaluators' scores were averaged for each condition. Depending on the number of groups, a one-way ANOVA or t-test was run. If the data were nonparametric, Kruskal- Wallis or Mann-Whitney were run.

Open Field Test

The Open Field test is used to determine exploration, general locomotor activity and anxiety, and animals were tested at approximately 6 MPT. A four-arena maze (each 40 cm x 40 cm) was used to analyze multiple animals at once. Animals were acclimated to the test room for at least one hour prior to the test. An animal was placed in the center of the open field and allowed to explore for five minutes and then returned to its home cage. Animals that experienced a generalized seizure during the test were returned to home cage and re-tested after 30 minutes if possible. Video was recorded using Media Recorder (Noldus) and analyzed using Ethovision XT (Noldus) software. The apparatus was cleaned between each animal using Nolvasan® solution to minimize odor cues. Animals were excluded from analysis if they rotated in one direction more than 10-times more

frequently than the other direction (<10% of the mice in Figure 7N). Evaluations included the total amount of time spent in the center of the maze, and velocity and distance traveled. Depending on the number of groups, a one-way ANOVA or t-test was used for statistical analysis. If the data were nonparametric, Kruskal-Wallis or Mann-Whitney tests were used for statistical analysis.

Barnes Maze Test

The Barnes Maze is a dry-land maze used to assess visual-spatial learning and memory in rats and mice, which is partially impaired in the focal kainate mouse model.[113] The maze is an elevated circular platform with a diameter of 92 cm. Twenty 5 cm holes line the edge of the maze and a hidden chamber is placed underneath one hole. Visual clues were placed around the room and lights acted as a mildly aversive stimulus. Acquisition and probe trials were video recorded using Media Recorder and analyzed using Ethovision XT software. On the first day of testing, animals were familiarized with the maze and hidden chamber. The animal was first placed in a red plastic, open-ended cylinder in the center of the maze and after 10 seconds the cylinder was removed. The animal could explore the maze for 2 minutes and after this time the animal was gently guided to the hidden chamber. Once in the chamber, the animal remained there for 1 minute before being returned to the home cage. This step was repeated one more time if animals were resistant to entering the hole. Acquisition trials were run on Days 1-3, and up to three trials were conducted each day. Animals were placed in the room 1 hour before the first trial for acclimation. Each animal had up to 3 minutes to find the hidden chamber and if it did not, the animal was gently guided to the hidden chamber after the time elapsed. The location of the hidden chamber remained the same for all animals during the acquisition trials. The maze and hidden chamber were cleaned between each animal using Nolvasan® solution to avoid odor cues. Animal order was randomized using Random.org. Experimenters were masked to the animal's treatment. Animals that experienced a generalized seizure during a trial were returned to home cage and retested after 30 minutes if possible. On Day 5 a probe trial was run. During this trial, the escape chamber was removed and each animal had up to 3 minutes to explore the maze. After 3 minutes, the animal was returned to its home cage. To assess long-term retention, an identical second probe trial was run approximately 10 days after the first probe trial. An animal's trial was excluded from analysis if the animal had a seizure during the trial, the animal was continuously circling, or if the animal fell off the maze more than twice during the trial. Animals were also excluded during probe trials if they didn't move more than 70 cm. We evaluated the number of errors and escape latency to the hidden goal box. A 2-way ANOVA was used for statistical analysis. If the data were nonparametric, Kruskal-Wallis or Mann-Whitney tests were used for statistical analysis.

Y-Maze

The Y-Maze alternation test is used to determine exploration and spatial memory and has been used in the literature for assessing effects of GABAergic transplants in epileptic mice.[45] The Y-Maze is a three-arm maze and each arm contains a visual cue. Animals were placed in the room 1 hour before the start of the test for acclimation. To begin the test, the animal is placed in the previously chosen "start" arm facing the center of the maze. The animal can explore for 5 minutes and is then returned to its home cage. Animals that experienced a generalized seizure during the test were returned to home cage and re-tested after 30 minutes. Video was recorded using Media Recorder and analyzed using Ethovision XT software. The maze was cleaned between each animal using Nolvasan® solution to avoid odor cues. Animals were tested once, usually at the end of the study. Animals would be excluded from analysis if they didn't enter each arm at least twice. Outcomes that were evaluated included the number of arms entered, percent of arms entered with alternation, and direction of alternation. Depending on the endpoint evaluated, a one-way ANOVA or t-test was used for statistical analysis. If the data were nonparametric, Kruskal-Wallis or Mann-Whitney tests were used for statistical analysis.

Perfusion

At the scheduled termination time point, animals were transcardially perfused with cold saline followed by 4% PFA. Brain tissue was collected and immersion fixed overnight in 4% PFA, followed by cryoprotection with 30% sucrose in phosphate buffered saline. For animals found dead, brain tissue was collected when possible.

EEG analysis

EEG was analyzed by researchers masked to treatment and group allocation either in-house or by the CRO SynapCell (St. Ismier, France). EEG that was not readable due to bad quality of the recording was not analyzed and the animal was excluded from the EEG endpoint. In-house EEG was analyzed using Neuroscore (DSI). The read-out for this model was focal electrographic seizures.[79,82,93,105,114] These ictal events were not present in sham-treated animals that did not receive an intrahippocampal kainate injection.[115] Electrographic seizures are defined as a synchronous activity with changes in spike frequency with a duration of at least 5 seconds at double the amplitude as baseline EEG. The inter-event interval was set at 1 second. In our hands, epileptic mice displayed around 11-15 electrographic seizures/30min early after SE in the MTLE model (Figure 3). The same experimenter read the EEG of the same animals at different time points post-transplant to limit variation. A 30-minute interval of EEG was analyzed for electrographic seizures each day for 7 consecutive days per time point. All EEGs were analyzed from the same time of day if possible (16:00). Since EEG traces can become increasingly hard to analyze with time after implantation of the electrodes, the following criteria were applied: (1) if no clean trace for a duration of 30 minutes was found, the next clean 30 minute interval within the next 3 hours was used; (2) if no 30 minute clean EEG stretch was found between 16:00-19:00, the EEG was read between 15:00-16:00; (3) it was confirmed that there were no generalized seizures, which occur rather infrequently in this model, in the hour before the 30-minute analysis interval, because post-ictal depression could confound the

results. If a seizure was seen, the analysis time window would be moved accordingly; and (4) if an event crossed the predicted start/end of the 30-minute reading interval, it would still be counted. Animals that did not show any seizure activity at baseline were excluded from the study.

RNA FISH

RNA fluorescence in situ hybridization (FISH) was performed on fixed, frozen mouse brain sections using RNAscope Multiplex Fluorescent Reagent Kit v2 Assay (Advanced Cell Diagnostics cat# 323100) according to the manufacturer's instructions. Briefly, 40 μm sections were post-fixed with 4% PFA and dehydrated with 50%, 70% and 100% ethanol. Sections were pretreated with hydrogen peroxide and target retrieval was performed. Following a 30-minute protease treatment, they were hybridized to probes targeting human GAD1 (Advanced Cell Diagnostics cat# 404031-C3) and human GAPDH, cross-validated not to recognize the mouse GAPDH gene (Advanced Cell Diagnostics cat# 442201-C2). Further amplification was performed according to the assay kit protocol, and Opal 520 (Akoya Biosciences cat# NC1601877) and Opal 690 (Akoya Biosciences cat# NC1605064) dyes were used to fluorescently label the probes. Tile scan images were acquired using the Leica DMi8 microscope. Analysis was performed manually using the Leica Application Suite X (LAS X) software and values represented are the percentage of human GAPDH-positive cells that express GAD1 in 2 sections for each of n=10 animals with Lot 1-U and n=8 animals with Lot 1-S.

Histology

Brain tissue through the HC was sectioned at 40 μm on a slide microtome or cryostat in 12 series of sections and processed for IHC and chromogenic tissue stains. All brain sections examined were assessed for the presence of ectopic tissue and development of micropathology. Analysis involved determining if the electrode and cell transplantations had been appropriately targeted within the HC, and persistence, distribution, and fate of transplanted human cells: One series of sections was stained with Nissl or H&E to identify any potential ectopic tissue or teratomas. Other tissue series were used to label for human cells (human nuclear antigen (HNA)), and several desired on-target markers such as LHX6, SST, PV, as well as off-target or proliferation markers such as DCX, GFAP, OLIG2, and KI67.

Measurement of GC dispersion width and area

Granule cell dispersion has been quantified by measurements of the GC layer width and area at -1.8 mm from Bregma, which is close to the site of kainate injection. The average GC layer width (manually defined at three set places during image analysis, illustrated by white lines in Figure 7B), and GC layer area (manually traced during image analysis, illustrated by the white boundary in Figure 7B) were quantified using Zen Blue.

QUANTIFICATION AND STATISTICAL ANALYSIS

Statistical analysis

For sample size calculations we used G*Power after initial experiments.[116] Analysis was performed using GraphPad Prism 9 (GraphPad). Data were first tested for normal distribution. Parametric data were tested by t-test when 2 groups were compared, and by ANOVA if 3 or more groups were compared. Non-parametric data were tested accordingly by Mann-Whitney test or Kruskal Wallis test. Post hoc tests were performed if analysis of variance revealed differences. The level of significance was set to p=0.05. Most data were plotted as mean ± SEM; behavior scores were plotted as median with interquartile range. EEG data were analyzed on a per animal basis and reported as the mean of electrographic seizures and seizures per recording period. To compare results across multiple studies, the mean seizure frequency of the vehicle group was normalized to zero at each respective time point, while the individual cell-transplanted and vehicle-injected animals were plotted as a percent difference in seizure frequency from the respective vehicle control group mean.

Randomization and masking

Experimenters were masked to the animals' treatment for the entire duration of the study and subsequent data analysis. During SE induction surgeries, 2-3 mice from each group cage were chosen randomly to distribute animals across all cages for a surgical day. All mice received the same treatment and were assigned a unique identifier number after surgery. For transplantation surgeries, mice were randomly selected from the holding rack (8 single-housed cages per row, per transplantation day at least 2 cages per row were selected). Treatment group allocation was only noted on surgery sheets and on an electronic database. Access to physical sheets and the database was limited to one person not involved in the study until the study was fully completed and all data were analyzed. The EEG files did not reveal the animal number. EEG was read on a per-channel basis by researchers who were masked to the treatment and animal identifier. The code for channel/animal number was kept at Neurona and not shared with the CRO. The CRO also had no information on the scope of the study, the treatment specifics or time points that they were analyzing. In-house data review was also performed in a masked manner and EEG traces did not contain information to allow identification of the animal number or treatment group. In behavioral studies, the experimenters remained masked to treatment groups throughout the study and the testing order was either random cage selection from the housing rack or assigned by using the website random.org. All histological processing

was done in a masked fashion by assigning the animals a new, coded identification prior to perfusion by a person not involved in the study. With these levels of masking in place, it was not possible to correlate EEG data with the histological analysis before all analyses were completed.

ADDITIONAL RESOURCES

The work presented here, using research-grade lots, represents the foundational research that led to IND-enabling studies in support of an ongoing Phase 1/2 clinical trial of NRTX-1001 in drug-resistant MTLE (https://www.clinicaltrials.gov/ct2/show/NCT05135091).